NOAA Technical Memorandum ERL WPL-91

METHODS FOR OBTAINING DAYTIME VERTICAL PROFILES OF C_n^2 AND WIND

G. R. Ochs
S. F. Clifford

Wave Propagation Laboratory
Boulder, Colorado
December 1981

noaa NATIONAL OCEANIC AND ATMOSPHERIC ADMINISTRATION / Environmental Research Laboratories

NOAA Technical Memorandum ERL WPL-91

METHODS FOR OBTAINING DAYTIME VERTICAL PROFILES OF C_n^2 AND WIND

G. R. Ochs
S. F. Clifford

Wave Propagation Laboratory
Boulder, Colorado
December 1981

UNITED STATES
DEPARTMENT OF COMMERCE
Malcolm Baldrige,
Secretary

NATIONAL OCEANIC AND
ATMOSPHERIC ADMINISTRATION
John V. Byrne,
Administrator

Environmental Research
Laboratories
George H. Ludwig
Director

This research was supported in part by the Defense Advanced Research Projects Agency of the Department of Defense, and was monitored by Donald O. Tarazano of the Rome Air Development Center, Griffiss Air Force Base, New York 13441, under Contract F30602-80-F-0248. Additional support was provided by the Air Force Geophysics Laboratory, Hanscom Air Force Base, Massachusetts 01731, under Project Order ESDI-0953, monitored by R. Earl Good.

TABLE OF CONTENTS

METHODS FOR OBTAINING DAYTIME VERTICAL PROFILES OF C_n^2 AND WIND

G.R. Ochs and S.F. Clifford

ABSTRACT

We report on an investigation of methods for profiling the refractive index structure parameter (C_n^2) and horizontal wind during daylight hours. The research effort has concentrated on the use of a solar scintillometer for this application.

INTRODUCTION

The goal of this research effort has been to devise a system for daytime measurement of clear air refractive-index turbulence effects as they apply to the propagation of an upwardly-directed laser beam. The atmospheric measurements required are nearly the same as those required for assessing astronomical image quality. A number of optical techniques have been suggested and employed for measuring atmospheric refractive turbulence effects.[1,2,3,4,5] An excellent recent discussion of the astronomical seeing problem with many references is contained in reference 5, where it is noted that Fried's parameter r_o can almost completely determine image quality. Ideally, however, a system should be capable of obtaining C_n^2 and wind profiles up through the tropopause, and be easily transportable for site survey purposes. Wind profiles, although of secondary importance, are also of interest as the information is important to the design of image compensating systems. The wind speed (v) is especially important when the product $C_n^2 v^{5/3}$ is large. An estimate of how this function varies with height is useful in determining what height ranges are the most important to measure.

The following procedure has been used to estimate the product $C_n^2 v^{5/3}$ as a function of height above ground. Hufnagel's model[7] was used as follows: For height Z above ground <3000 meters,

$$C_n^2 = C_{n_1}^2 Z^{-4/3}$$

where $C_n^2 = C_{n_1}^2$ at Z = 1 meter. For $Z \geq 3000$ meters,

$$C_n^2 = \{[(2.2\text{x}10^{-53})Z^{10}(W/27)^2]\exp(-Z/1000)+(10^{-16})\ \exp(-Z/1500)\}\ 2.7$$

where

Z = meters above sea level,

W = average wind speed from Z = 5 to 15 km.

A Gaussian wind-height function was chosen of the form

$$v = A+(B-A)\exp[-|Z-Z_1|/Z_2]$$

where

A = Wind speed at Z = 0,

B = maximum wind speed at height Z_1,

Z_2 = height spread to $\pm$ v/e.

A result for $C_{n_1}^2 = 10^{-12}$

A = 5 m/s

B = 50 m/s

Z_1 = 7000 m

Z_2 = 5000 m

is shown in Table I.

An examination of the cumulative sum of $C_n^2\ v^{5/3}$ shows that 0.5 of the effect is below 3000 meters and 0.9 is below 9000 meters. Some other results are tabulated in Table II. In general it appears that even for high jet stream winds (50 - 150 m/s), a measurement to 10 km is adequate. For 10 m/s, 5 km may be adequate. Another consideration is the degree of freedom available in the site selection process. One would not expact to find statistical variations in C_n^2

Table I

E	V	CN↑2E18	CN↑2E18*V↑(5/3)	CUM. SUM
1	5.00294	9.99998E-13	1.46344E-11	1.46344E-11
2	5.0059	3.9685E-13	5.81337E-12	2.04478E-11
3	5.00884	2.31121E-13	3.38895E-12	2.38367E-11
4	5.01179	1.5749E-13	2.31157E-12	2.61483E-11
5	5.01474	1.16961E-13	1.71838E-12	2.78667E-11
6	5.01769	9.17203E-14	1.34887E-12	2.92155E-11
7	5.02064	7.46802E-14	1.09935E-12	3.03149E-11
8	5.02359	6.25E-14	9.20948E-13	3.12358E-11
9	5.02654	5.34167E-14	7.87875E-13	3.20237E-11
10	5.02949	4.6416E-14	6.85288E-13	3.2709E-11
20	5.05903	1.84202E-14	2.74624E-13	3.54552E-11
30	5.08864	1.07277E-14	1.61501E-13	3.70702E-11
40	5.1183	7.31007E-15	1.11121E-13	3.81814E-11
50	5.14803	5.42885E-15	8.33249E-14	3.90147E-11
60	5.17781	4.2573E-15	6.59745E-14	3.96744E-11
70	5.20765	3.46634E-15	5.42342E-14	4.02168E-11
80	5.23756	2.901E-15	4.58242E-14	4.0675E-11
90	5.26752	2.4794E-15	3.95386E-14	4.10704E-11
100	5.29754	2.15444E-15	3.46836E-14	4.14172E-11
200	5.6011	8.54991E-16	1.51036E-14	4.29276E-11
300	5.91079	4.97936E-16	9.62161E-15	4.38897E-11
400	6.22674	3.39304E-16	7.1508E-15	4.46048E-11
500	6.54906	2.51986E-16	5.77661E-15	4.51825E-11
600	6.8779	1.97606E-16	4.91537E-15	4.5674E-11
700	7.21338	1.60894E-16	4.33278E-15	4.61073E-11
800	7.55564	1.34653E-16	3.9174E-15	4.6499E-11
900	7.90482	1.15084E-16	3.60992E-15	4.686E-11
1000	8.26104	1.00001E-16	3.37592E-15	4.71976E-11
2000	12.2441	3.96853E-17	2.5813E-15	4.97789E-11
3000	17.109	3.66942E-17	4.16839E-15	5.39473E-11 ← .5
4000	23.051	1.97644E-17	3.69003E-15	5.76373E-11
5000	30.3085	1.30715E-17	3.8512E-15	6.14885E-11
6000	39.173	1.27797E-17	5.77428E-15	6.72628E-11
7000	50	1.60027E-17	1.08594E-14	7.81222E-11
8000	39.173	2.0132E-17	9.09626E-15	8.72184E-11
9000	30.3085	2.3162E-17	6.82413E-15	9.40426E-11 ← .9
10000	23.051	2.40748E-17	4.49479E-15	9.85373E-11
11000	17.109	2.28198E-17	2.59229E-15	1.0113E-10
12000	12.2441	1.99765E-17	1.29935E-15	1.02429E-10
13000	8.26104	1.63346E-17	5.51438E-16	1.0298E-10
14000	5	1.25959E-17	1.84153E-16	1.03165E-10
15000	2.33009	9.23269E-18	3.78108E-17	1.03202E-10
16000	.14415	6.4741E-18	2.56569E-19	1.03203E-10

Table II

Ground wind speed	Max. m/s	Wind speed height m	Wind speed spread	C_n^2 at 1 m	0.5 atmosphere height, m	0.9 atmosphere height, m
5	50	7000	5000	10^{-12}	3000	9000
5	50	7000	5000	10^{-13}	7000	10000
5	100	7000	5000	10^{-12}	7000	9000
1	50	7000	5000	10^{-12}	6000	9000
1	10	7000	5000	10^{-12}	10	5000
5	50	7000	10000	10^{-12}	6000	10000
5	50	7000	10000	10^{-13}	2000	10000

levels at high altitude between sites, say, less than 10 km apart, except perhaps at locations downwind of mountain ranges. On the other hand marked differences in low altitude C_n^2 could occur with sites just tens of meters apart. A summary of an extensive series of measurements of importance to site selection made above the high desert and mountain terrain of the White Sands Missile Range, New Mexico, is contained in references 8 and 9. Generally it is found that mountain sites are superior at night but about the same as desert floor locations in the daytime. Most of the differences between sites arise from atmospheric differences in the first 100 meters above local terrain. There is some radar evidence, however, that daytime high altitude C_n^2 can be quite variable from day to day.[10]

Various techniques are available or could possibly be developed for daytime profiling of C_n^2. Some of these are listed below:

Radiosondes with high-speed temperature sensors
Airplanes with high-speed temperature sensors
Radar, low frequency, pulsed
Radar, frequency-modulated continuous wave
Acoustic sounder
Optical scintillometer (the NOAA C_n^2 meter)
Stellar scintillations
Lidar
Edge-of-sun scintillations
Full-sun scintillations

All but the last three techniques are in use, and quite satisfactory for many applications. Some comments about their suitability in this application follow.

Radiosonde-mounted high-speed temperature probes have been used for some years to measure the temperature structure parameter (C_t^2), from which C_n^2 can be derived. Their chief disadvantages arise from the intermittent measurement, the likely loss of equipment on each flight, and the manpower needed for each launch. However, altitude resolution is good, high altitude measurements are possible, and they can be launched at any time. We have developed and flown a low-priced C_t^2 meter during this contract and have obtained satisfactory C_n^2 profiles from it. A separate report describes this instrument.[11]

We have also flown high-speed temperature probes mounted on aircraft.[12] Our system design is available but it is very much a custom installation for the particular aircraft used. Intermittent operation, cost, and reduced signal-to-noise at high altitudes due to the aircraft environment, are disadvantages.

Radar techniques can measure C_n^2 but include the water vapor component. However this is not very important at high altitudes. The pulsed low-frequency radars work well at high altitudes but are major non-portable installations. The frequency-modulated continuous wave radars can be a portable operation. They operate at lower altitudes, however, where the water vapor contribution to C_n^2 is significant.

Acoustic sounders are proven devices for measuring C_n^2 in the lower atmosphere. They have good altitude resolution, are relatively inexpensive, and are commerically available, but the height range is limited to about 600 meters.

The NOAA C_n^2 meter is a good device for obtaining path-averaged C_n^2 measurements. Since it is a two-ended system it is not suitable for vertical profiling, but might well be used as a supplementary measurement near the ground. We have installed three systems operating on slant paths to the Boulder Atmospheric Observatory tower to compare with readings from the solar scintillometer.

D. L. Walters has developed an instrument that derives the transverse coherence length (r_o) from star trail photographs.[13] This device operates both day and night and while it does not obtain a vertical profile of C_n^2, the value of r_o is directly related to the atmospheric effect upon an upwardly-directed laser beam, measuring over the entire altitude range. The data reduction requires analysis of star trail photographs. Recently, however, the instrument has been redesigned so that on-line data analysis is available, making this method very attractive.[14] Another possibility is to convert the NOAA star scintillometer to operate on stars in the daytime. This should be possible with somewhat reduced signal-to-noise, using a system to correct for the background sky-light contamination, and a high quality servo-controlled tracking system. The disadvantages are the observatory-type installation required and the inability to measure below 2 km above the ground. Where an alternate method does not measure well at high altitude, however, the simpler arrangement of observing log-amplitude variance (σ_χ^2) over a 10 to 20 cm

diameter aperture might be used to supplement a lower altitude measurement. Additionally, Loos and Hogge[15] have pointed out that under low turbulence conditions there is a good correlation between σ_χ^2 for a 10 cm diameter objective observing a star, and the isoplanatic angle. They show that the σ_χ^2 weighting function for this diameter is very close to the isoplanatic weighting function. A seeing monitor of this type would have many advantages. It could operate nearly continuously on bright stars day and night and be able to process the data on line. A differencing system would have to be devised to cancel out the background light in the daytime, however. The measurement would ignore effects very near the instrument. This might well be an advantage. While this portion of the path has a very real effect upon seeing, it is influenced to a great extent by the instrument mounting arrangement, rather than the undisturbed atmosphere very near the ground.

One approach to daytime measurements of C_n^2 profiles is to use a lidar technique that we have invented, based on previous work with diffraction-limited Doppler lidars. Briefly stated, a single-mode laser transmitter is used to illuminate a region of the atmosphere at a height selected by time-gating the return from a pulsed laser. Molecular scattering creates an illuminated target, with dimensions determined by the diffraction limit of the transmitting optics in the absence of any imhomogeneities in atmospheric refractive index. Refractive turbulence will spread the illuminated region beyond the diffraction limit. By measuring the dimensions of the lidar image we can determine the effect of C_n^2 on the light propagated to the sample height and back, and by making measurements at different altitudes we can determine a profile of C_n^2. The status of research on this idea is that we are currently involved in a computer simulation of the performance of such a lidar with modest dimensions, suitable for mobile deployment in a light vehicle. We intend to determine if such a lidar will have enough image spread to generate C_n^2 profiles to 10 or 20 km with useful signal-to-noise in a few minutes integration time. If the results of the simulation are promising, the next step is to construct a field test system. One useful aspect of a C_n^2 lidar is that it makes measurements in a mode similar to that employed in a laser communications uplink.

In principle it is possible to look at the angular fluctuations on the edge of the sun to obtain C_n^2 profiles. Pertinent work is described in references 16 and 17. We performed some experiments on a horizontal 500 m path on Table Mountain, using the experimental arrangement shown in Fig. 1. The light source was

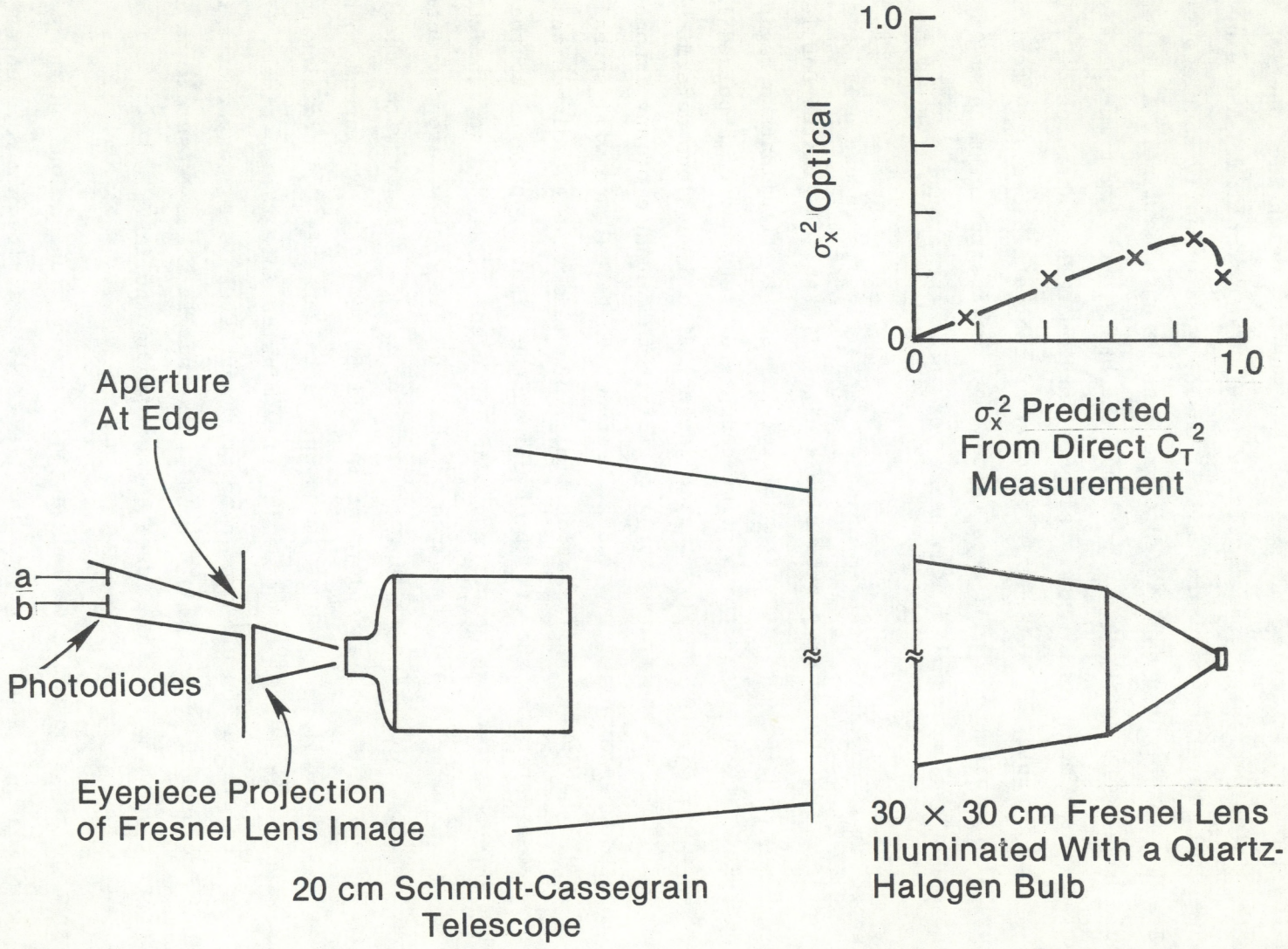

Figure 1. Edge effect experiment.

a 30 cm square Fresnel lens illuminated with a quartz-halogen lamp. An image of the Fresnel lens was formed by eyepiece projection from a 20 cm diameter Schmidt-Cassegrain telescope. An aperture was placed on the edge of this image that defined a 400 μrad field of view. Two photodiodes were placed behind this aperture. This arrangement converts angular fluctuations of the phase front at the telescope aperture to intensity fluctuations in the plane of the photodiodes. This particular geometry should emphasize fluctuations in the region of the center of the light path. Time-delayed fluctuations were observed by the photodiodes. We compared the function $(a-b)^2/ab$ with a direct measurement of C_t^2 with differential thermometers and obtained the relationship shown. The scales are arbitrary. Even with the fixed path, vibrations turned out to be a severe problem. Also it is not clear how a stable calibration could be set up and maintained for the measurement of C_n^2. To use this method, an observatory-type installation would be required.

Another possibility is to examine the contrast of the solar granulations and derive r_o from this observation.[5] Apparently, there is some difficulty in evaluating the effects of scattered light, however.

The full-sun scintillation technique was finally chosen for a more extensive theoretical and experimental study. Some small-aperture solar scintillation measurements were reported in 1971[18] and a derivation explaining the variance and the correlation function of solar-flux scintillations is contained in reference 19. Our preliminary analysis and experiments were promising. While large apertures would be required to measure at high altitudes, these could be formed inexpensively by measuring the irradiance by the sun of flat areas on the ground. Tracking mounts would not be required and rather simple detectors could be used. Some difficulties were expected, however, because the log-amplitude variance (σ_χ^2) of the irradiance would be quite small, especially for the high altitude measurement.

THEORY OF SOLAR SCINTILLATION

For spatially incoherent sources it is not difficult to show that the time-lagged covariance of the fluctuations in log-amplitude of two detectors spaced a displacement $\underset{\sim}{\rho}$ has the form[20]

$$C_\chi(\underset{\sim}{\rho},\tau) = 2\pi k^2 \int_0^L dz' \int d^2\underset{\sim}{K}\, e^{i\underset{\sim}{K}\cdot\underset{\sim}{\rho}z'/L - i\underset{\sim}{K}\cdot\underset{\sim}{V}\tau} \sin^2\left[\frac{K^2 z'(L - z')}{2kL}\right] \Phi_n(\underset{\sim}{K},z')$$

$$F(\underset{\sim}{K}\, z'/L)\; G[\underset{\sim}{K}(1 - z'/L)]\;, \qquad (1)$$

where $k = 2\pi/\lambda$, λ is the wavelength of light impinging upon the detectors, Φ_n is the locally homogeneous spectral density of the refractive index fluctuations, $\underset{\sim}{K}$ is the two-dimensional spatial wavenumber, $\underset{\sim}{V}$ is the velocity vector transverse to the line-of-sight to the source, z' is the distance from the transmitter along the propagation path of total length L, τ is the differential time-lag of the signals from the detectors and F and G are, respectively, the power spectral densities of the receiver apodization and transmitter amplitude distribution normalized to unity at $K = 0$. We may specialize this result to the solar scintillation case by noting in this problem that the refractive turbulence is compressed very close to the receiver so that $z'/L \sim 1$. Making the convenient change of variables to the height above ground $z = L - z'$, we have

$$C_\chi(\underset{\sim}{\rho},\tau) = 2\pi k^2 \int_0^L dz' \int d^2\underset{\sim}{K}\, e^{i\underset{\sim}{K}\cdot[\underset{\sim}{\rho}-\underset{\sim}{V}\tau]} \sin^2\left[\frac{K^2 z}{2k}\right] \Phi_n(\underset{\sim}{K},z)\; F(\underset{\sim}{K})\; G(\underset{\sim}{K}\, z/L)\;. \qquad (2)$$

The spectrum Φ_n for locally homogeneous, isotropic refractive turbulence in the inertial subrange is from Tatarski[21]

$$\Phi_n(\underset{\sim}{K},z) = 0.033\, C_n^2(z)\, K^{-11/3}\;. \qquad (3)$$

If the detectors are uniform apertures of diameter D then

$$F(\underset{\sim}{K}) = F(K) = \left[\frac{2\, J_1(K\, D/2)}{(K\, D/2)}\right]^2\;. \qquad (4)$$

A similar function applies to the solar source if we ignore the small effect due to solar limb darkening; namely,

$$G(\underset{\sim}{K}\, z) = G(K\, z) = \left[\frac{2\, J_1(K\, z\, D_s/2L)}{(K\, z\, D_s/2L)}\right]^2 \qquad (5)$$

where J_1 is the first order Bessel function of the first kind and D_s is the solar diameter. If $D >> \sqrt{\lambda L}$ the function F(K) will fall off sufficiently fast in the important region of integration over K in (2) that the sine function may be replaced by its argument. Note that the atmosphere takes up a trivial fraction of the distance L to the sun, we may set $L = \infty$ in (2), integrate $d^2\underset{\sim}{K}$ over angle and obtain

$$C_\chi(\underset{\sim}{\rho},\tau) = 0.033\pi^2 \int_o^\infty dz\, z^2\, C_n^2(z) \int_o^\infty dK\, K^{4/3}\, J_o(K|\underset{\sim}{\rho}-\underset{\sim}{V}\tau|)$$

$$\left[\frac{2\, J_1(K\, D/2)}{(K\, D/2)}\right]^2 \left[\frac{2\, J_1(K\theta_s z/2)}{(K\theta_s\, z/2)}\right]^2 . \qquad (6)$$

where θ_s is the angle subtended by the solar diameter ($\theta_s \sim 0.0093$ rad).[22]

C_n^2 PROFILING

The simplest parameter to measure that contains information about C_n^2 is the single aperture variance $\sigma_\chi^2 = C_\chi(0,0)$. Letting $\underset{\sim}{\rho} = \underset{\sim}{0}$, $\tau = 0$ in (6), we obtain

$$\sigma_\chi^2 = 0.033\pi^2\, 2^{7/3}\, D^{2/3}\, \theta_s^{-3} \int_o^\infty dy\, C_n^2\, (y\, D/\theta_s)\, y^2 \int_o^\infty dx\, x^{4/3}$$

$$\left[\frac{2\, J_1(x)}{x}\right]^2 \left[\frac{2\, J_1(xy)}{(xy)}\right]^2 \qquad (7)$$

where we have let $y = z\theta_s/D$ and $x = K\, D/2$. To compute a rough estimate of the calibration coefficient we make a C_n^2 profile assumption of the plausible form $C_n^2(z) = C_{n_o}^2\, (z/z_o)^{-4/3}$. This form is valid for the boundary layer, but severely underestimates the effect of high altitude refractive turbulence. Inserting this profile in (7) and performing the necessary numerical integrations, we obtain for $C_n^2(z_o)$,

$$C_n^2(z_o) = C_{n_o}^2 = 0.17\, D^{2/3}\, \theta_s^{5/3}\, z_o^{-4/3} . \qquad (8)$$

Equation (8) relates the observed variance to the value of C_n^2 at $z = z_o$ assuming the $z^{-4/3}$ behavior of the C_n^2 profile. To see how an arbitrary profile is weighted when you observe scintillation, we calculate the so-called C_n^2 weighting function W(z) defined by the relation

$$\sigma_\chi^2 = \int_o^\infty dz\, C_n^2(z)\, W(z) \,, \tag{9}$$

where W(z) is the relative effectiveness of refractive turbulence at producing scintillation when located at a height z. From (6), again with $\underset{\sim}{\rho} = \underset{\sim}{0}$, $\tau = 0$, the result is

$$W(z) = 1.64\, D^{-7/3}\, z^2 \int_o^\infty dx\, x^{4/3} \left[\frac{2\, J_1(x)}{x}\right]^2 \left[\frac{2\, J_1(x\, \theta_s\, z/D)}{(x\, \theta_s\, z/D)}\right]^2 . \tag{10}$$

Equation (10) is plotted in Fig. 2 where we see a rather broad maximum located at approximately $2 - 3\ \theta_s/D$. (Note that unimportant factors independent of z have been dropped from (1) and will be dropped in weighting function calculations below.)

To reach higher altitudes 3 km, say, it is clear from Fig. 2 that rather large apertures $D \sim 10$ m must be used. To circumvent this problem we can measure the covariance function of two adjacent apertures which will push the peak weighting up higher. The covariance of two apertures separated by a distance ρ, $C_\chi(\rho)$, is $C_\chi(\underset{\sim}{\rho},0)$ from (6). The covariance weighting function, $W_c(\underset{\sim}{\rho},z)$, that is defined by

$$C_\chi(\rho) = \int_o^\infty dz\, W_c(\underset{\sim}{\rho},z)\, C_n^2(z) \tag{11}$$

is given by the expression

$$W_c(z) = 1.64\, D^{-7/3}\, z^2 \int_o^\infty dx\, x^{4/3}\, J_o(2x\rho/D) \left[\frac{2\, J_1(x)}{x}\right]^2 \left[\frac{2\, J_1(x\theta_s z/D)}{(x\theta_s\, z/D)}\right]^2 \tag{12}$$

This result is plotted for tangent apertures $\rho = D$ in Fig. 3. This figure illustrates that the peak has moved up significantly from $3\theta_s/D$ to $6\theta_s/D$ but also shows a serious problem with this approach; namely, a negative sidelobe at low altitudes. Because C_n^2 has larger values at lower heights, this effect could seriously reduce overall variance and prevent accurate profiling. A solution is

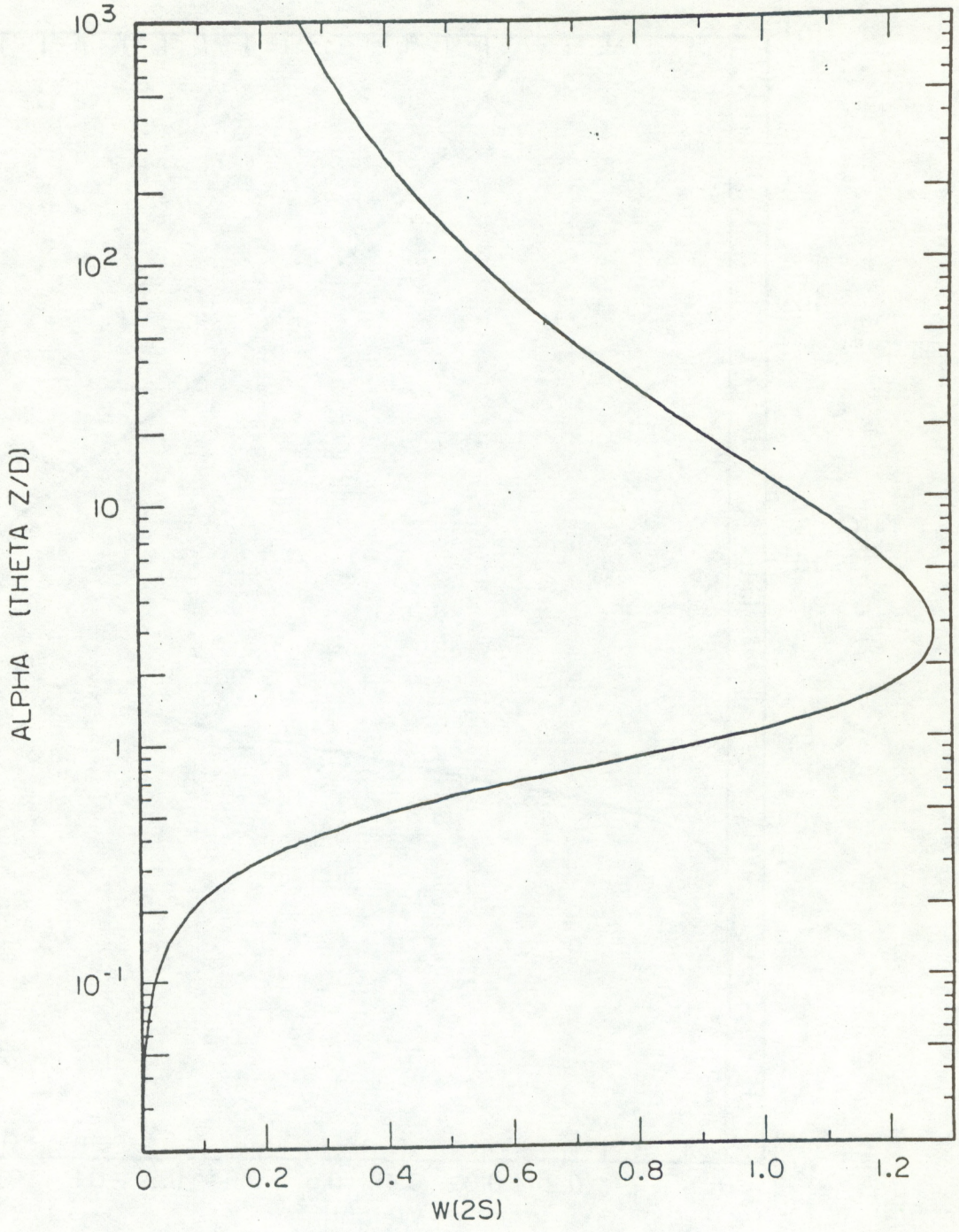

Figure 2. Weighting function for single-aperture variance. Beta = 0.

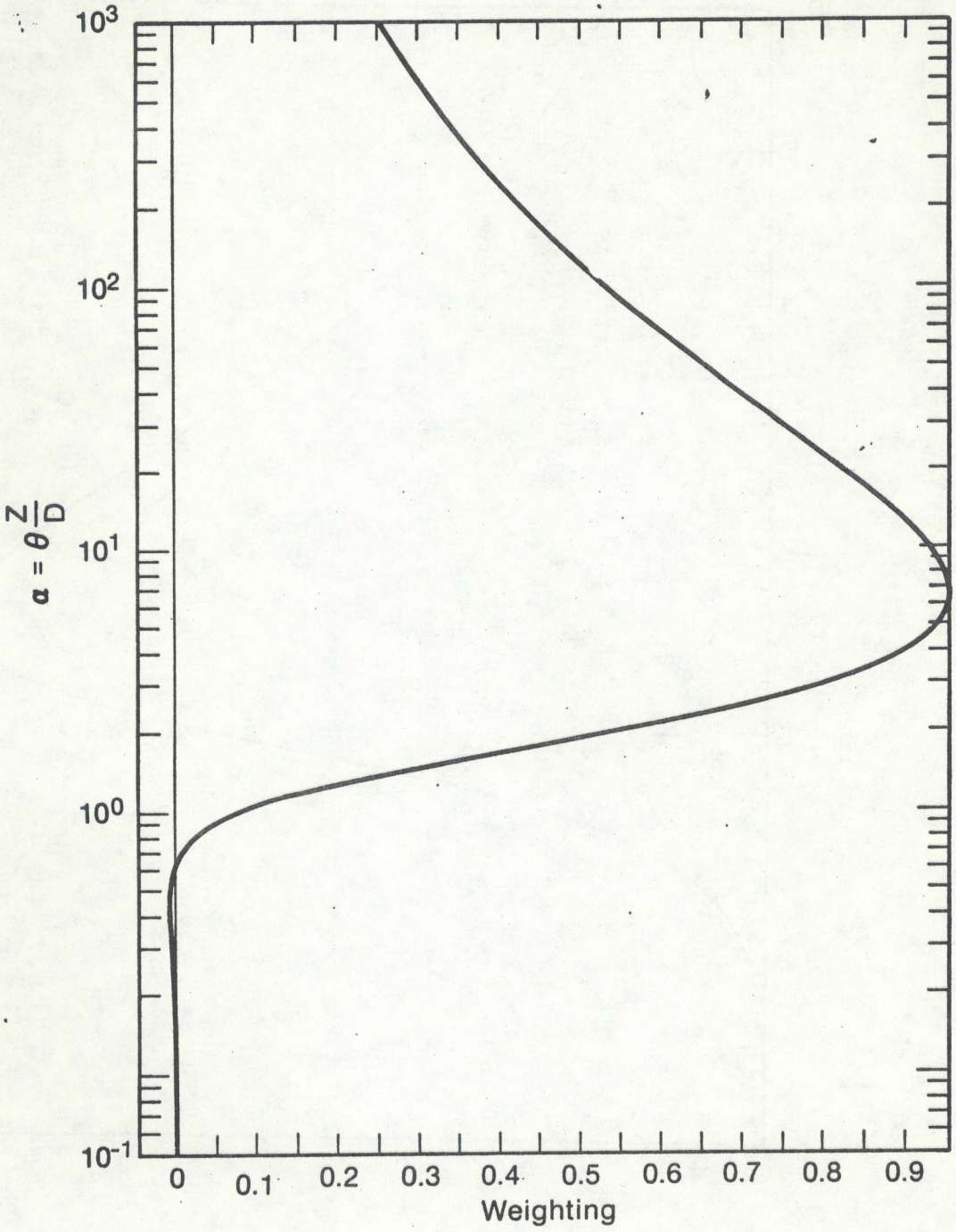

Figure 3. Weighting function for covariance of tangent apertures. Beta = 2.0.

to slightly overlap the effective apertures. We have determined numerically that $\rho = 0.85\ D$ is the optimum overlap that reduces the negative part to zero yet maintains sufficient separation to have reasonably independent scintillation measurements.

To improve spatial resolution and low spatial frequency noise rejection it is sometimes useful to use linear combinations of aperture signals. The most common of these arrays is the difference of two detectors whose weighting function $W_2(z)$ is defined by

$$W_2(z) = 3.28\ D^{-7/3}\ z^2 \int_0^\infty dx\ x^{4/3} \left[1 - J_o(2x\ \rho/D)\right] \left[\frac{2\ J_1(x)}{x}\right]^2 \left[\frac{2\ J_1(x\theta_s\ z/D)}{(x\theta_s\ z/D)}\right]^2 \quad (13)$$

and plotted in Fig. 4 for the case of tangent apertures $\rho = D$. Another useful array is the sum and difference of four apertures equally spaced a distance ρ apart, that is, if the four apertures are labeled successively A,B,C,D, then the measured quantity would be $\langle (A-B)(C-D) \rangle$, where the angle brackets indicate an ensemble average. This weighting function $W_4(z)$, defined by

$$W_4(z) = 1.64\ D^{-7/3}\ z^2 \int_0^\infty dx\ x^{4/3} \left[J_o(2x\rho/D) - J_o(6x\rho/D)\right] \left[\frac{2\ J_1(x)}{x}\right]^2 \left[\frac{2\ J_1(x\theta_s\ z/D)}{(x\theta_s\ z/D)}\right]^2 \quad (14)$$

is plotted for tangent apertures in Fig. 5. Note that in both cases the peak is considerably narrower and somewhat lower than the single aperture variance $W(z)$.

WIND PROFILING

Another feature of solar scintillation is the possibility of wind profiling by observing the drift of the solar scintillation pattern. Using two or more spaced sensors, the time for the pattern to drift across the array is related to the wind velocity component parallel to the array displacement vector. A linear technique for obtaining wind is estimating the slope of the log-amplitude covariance

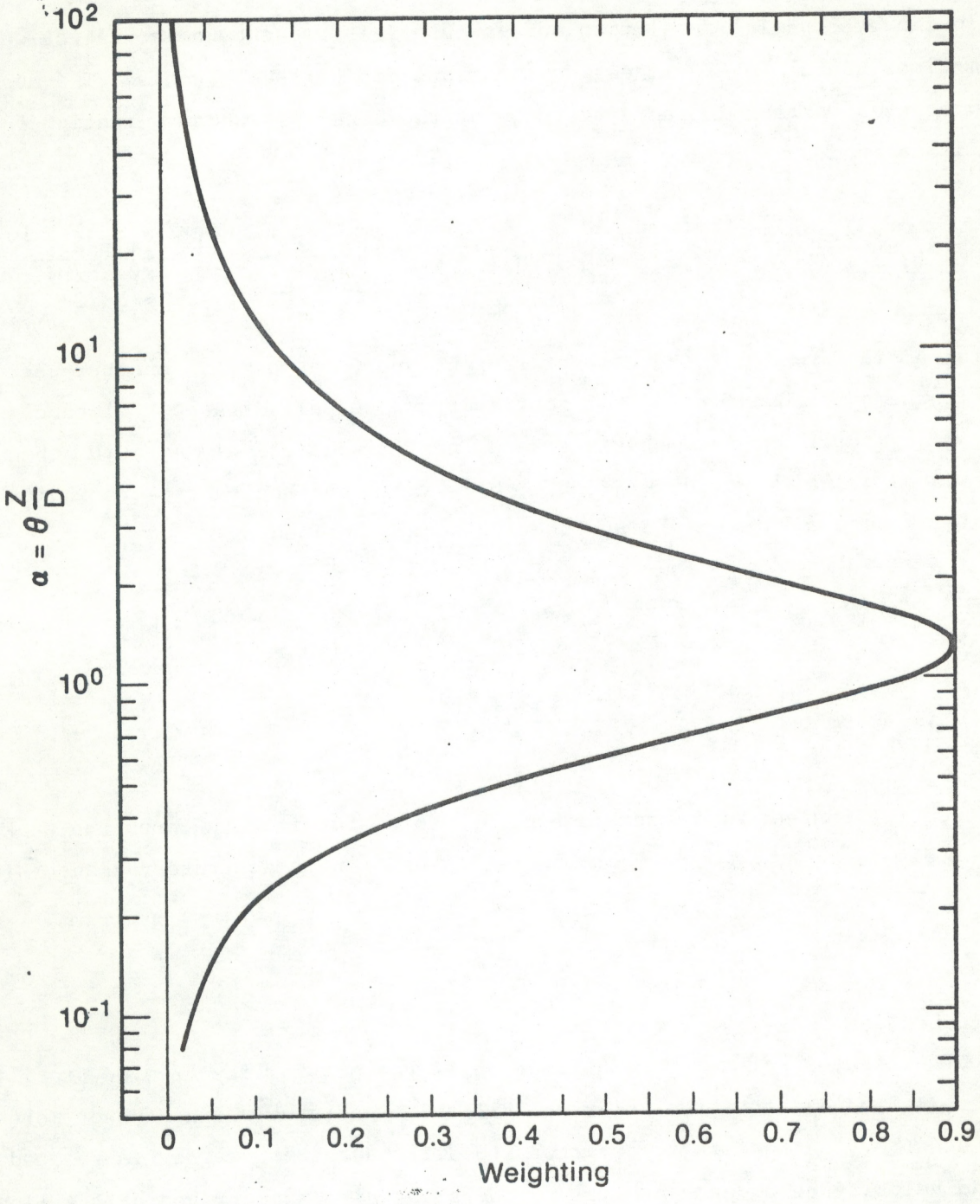

Figure 4. Weighting function for the variance of the difference of two apertures.

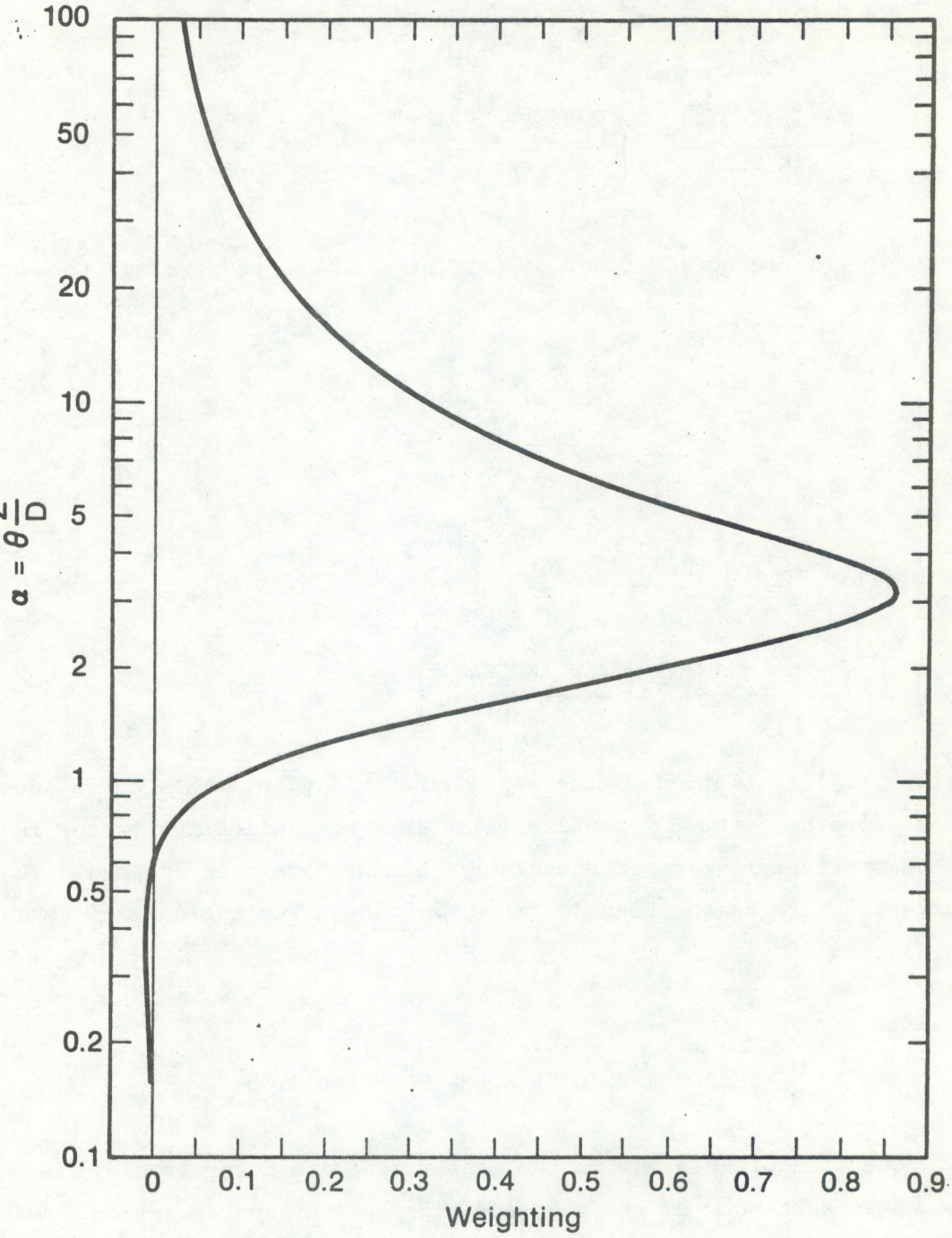

Figure 5. Weighting function for the variance of the difference of four apertures.

function at zero time lag.[23] From (6), we have for two apertures of diameter D separated by $\underset{\sim}{\rho}$, the expression

$$m = \left.\frac{\partial C_\chi}{\partial \tau}\right|_{\tau=0} = 0.033\pi^2 \int_o^\infty dz\, z^2\, C_n^2(z) \int_o^\infty dK\, K^{7/3}\, (\hat{\underset{\sim}{\rho}}\cdot\underset{\sim}{V})\, J_1(K\rho)$$

$$\left[\frac{2\, J_1(K\, D/2)}{(K\, D/2)}\right]^2 \left[\frac{2\, J_1(K\theta_s z/2)}{(K\theta_s z/2)}\right]^2 \qquad (15)$$

where $\hat{\underset{\sim}{\rho}} = \underset{\sim}{\rho}/\rho$. The weighting function for the wind component along the array $V_\perp$ is defined by

$$m = \int_o^\infty dz\, V_\perp(z)\, W_v(z) \qquad (16)$$

where from (15)

$$W_v(z) = 3.28\, D^{-10/3}\, z^2\, C_n^2(z) \int_o^\infty dx\, x^{7/3}\, J_1(2x\rho/D)$$

$$\left[\frac{2\, J_1(x)}{x}\right]^2 \left[\frac{2\, J_1(x\theta_s z/D)}{(x\theta_s z/D)}\right]^2 . \qquad (17)$$

Equation (17) is plotted as the solid line in Fig. 6. This curve does not contain the effects of the C_n^2 profile which is a multiplicative factor in (17). Also, the unimportant factors independent of height have been dropped. The dashed curve illustrates the behavior of $W_v(z)$ when a realistic $z^{-4/3}$ behavior of C_n^2 is assumed.

MEASUREMENTS OF SOLAR SCINTILLATION

The frequencies of interest in the measurement are determined by the wind speed, the angle subtended by the sun, and the receiver configuration. While at each altitude a range of spatial irregularity sizes contribute to the signal, it is useful to calculate the predominate spatial wavelength versus altitude. The result is shown in Fig. 7. We obtain this result by finding the $K_{max} = 2\pi/\ell_{max}$

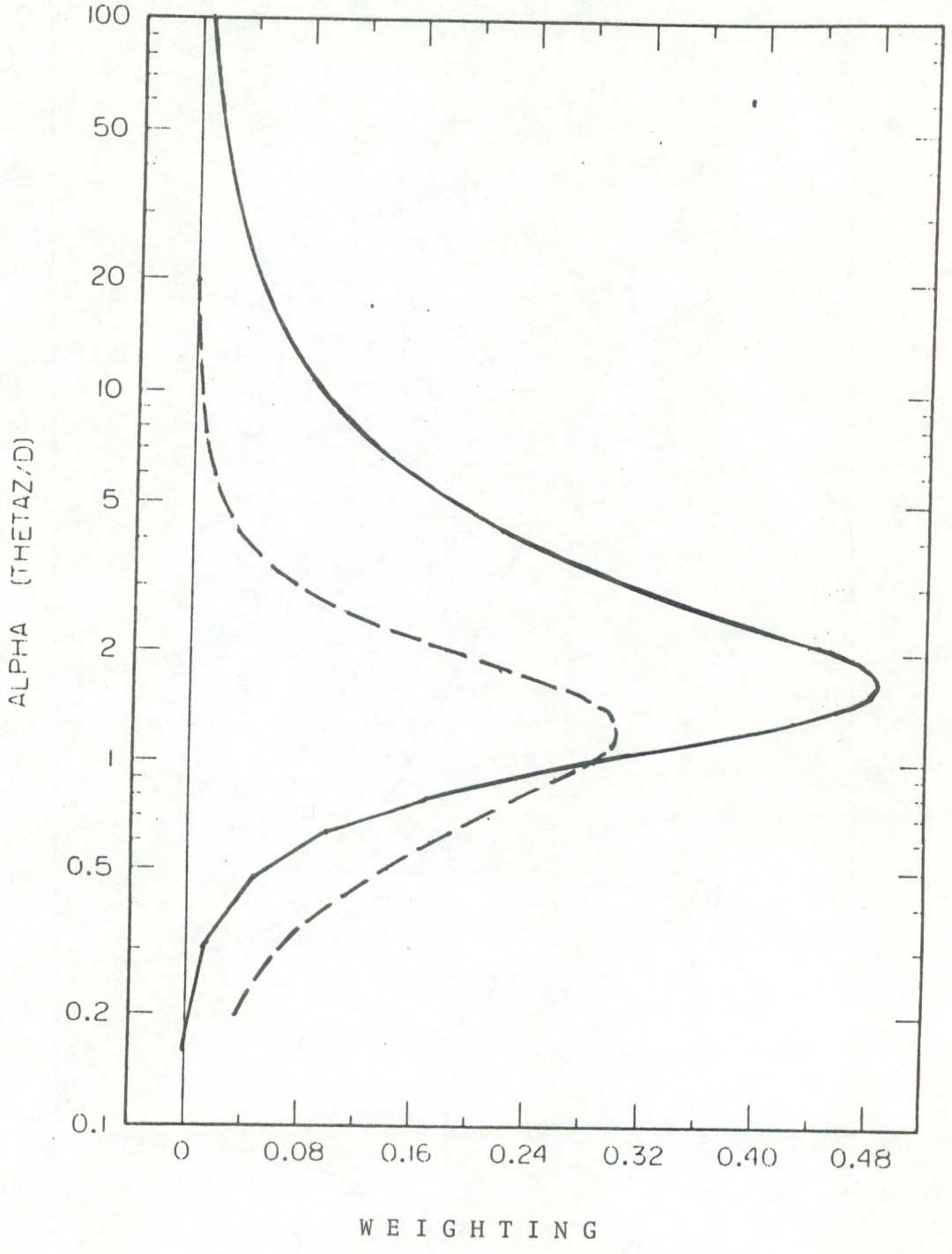

Figure 6. Wind weighting function for tangent apertures. The dashed line includes the effect of C_n^2 weighted according to $Z^{-4/3}$.

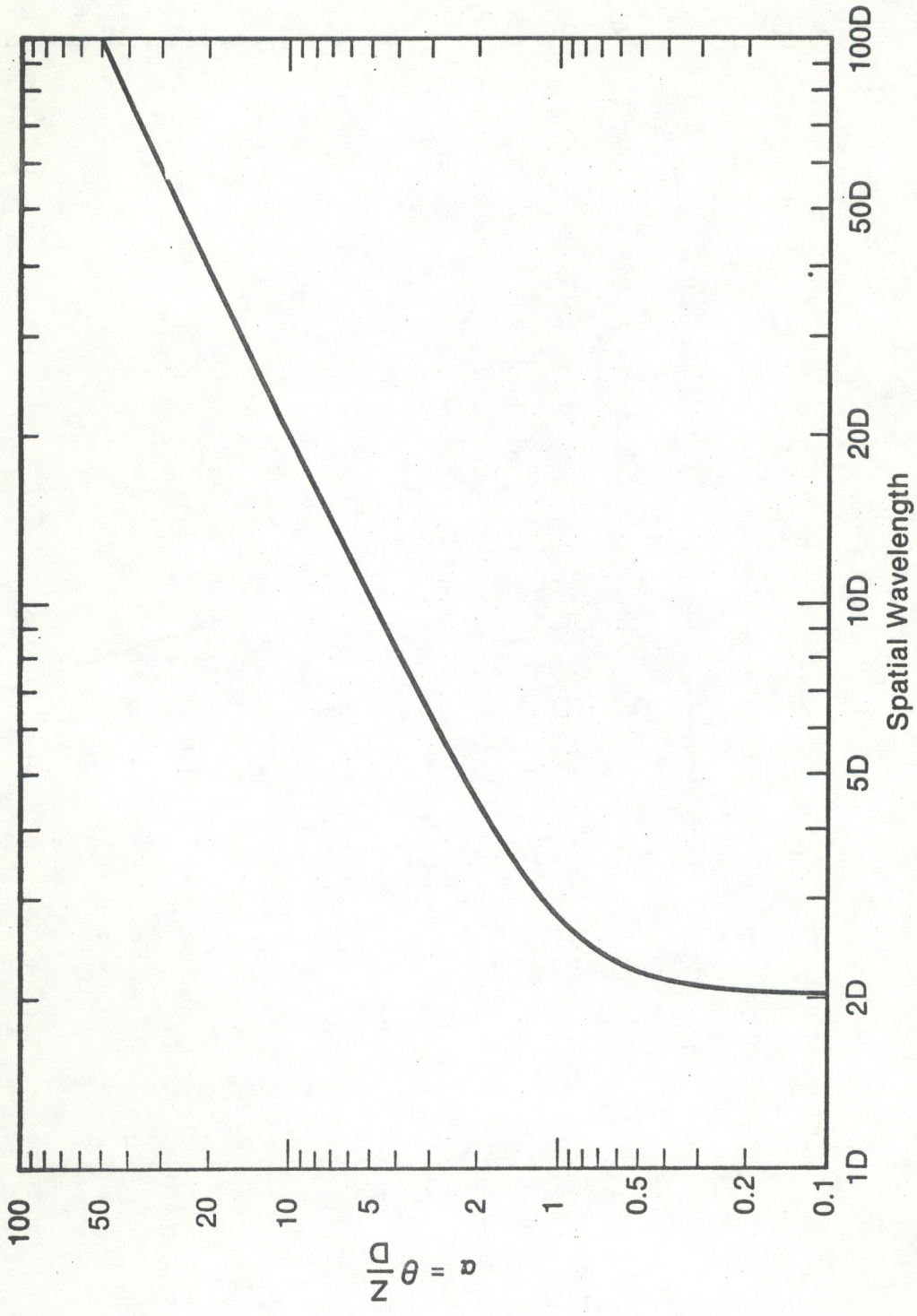

Figure 7. Spatial wavelength versus normalized altitude.

that maximizes the K integrand in Eq. (6) with ρ and τ set to zero. Figure 7 is a plot of ℓ_{max}. Note that the spatial wavelength is close to 2D at low altitude but starts to become larger somewhat below the peak of the C_n^2 and wind weighting functions. After the peak response, the spatial wavelength becomes nearly proportional to the height above ground. From these considerations, we chose a bandwidth from 0.1 to 160 Hz for the following experiments.

The arrangement shown in Fig. 8 was used to define a circular area on a piece of composition board or in some cases a concrete sidewalk. A photodiode 0.5 cm in diameter was placed in the focal plane of a 1-cm focal length lens, so that the diameter of the area observed was one-half the detector board distance. Aperture arrays were formed by using multiple sets of these. Because σ_χ^2 is very small, a preamplifier was designed and built (Fig. 9) which employs a servo loop to maintain a zero mean at the signal output. A second output provides a measure of the current required for balance. In this way the signal-to-noise is improved since only the fluctuating signal current flows through the first amplifier stage. The half-power rolloff frequency f_c of the high-pass filter formed by this arrangement occurs approximately at $f_c = G/2\pi RC$, where $G = r_1/r_2$. For the present circuit, $f_c = .1$ Hz.

If $\sigma_\chi^2 << 1$,

$$\sigma_\chi^2 = \frac{1}{4}\left[\frac{\overline{(I - \bar{I})^2}}{\bar{I}^2}\right] \tag{18}$$

where I is the irradiance of the aperture. This can be rewritten in terms of the preamplifier output V_{ac} and V_{dc} as

$$\sigma_\chi^2 = \frac{1}{4}\left[\frac{V_{ac}}{G\,V_{dc}}\right]^2 . \tag{19}$$

A plot of σ_χ^2 vs. time for various aperture diameters is shown in Fig. 10.

To calculate C_n^2 from σ_χ^2 for a single aperture, we use Eq. (8). According to the theory, if $C_n^2 \propto Z^{-4/3}$, then $\sigma_\chi^2 \propto D^{-2/3}$. In Fig. 11, we plot σ_χ^2 versus D from experimental data taken during unstable conditions. Lines are drawn

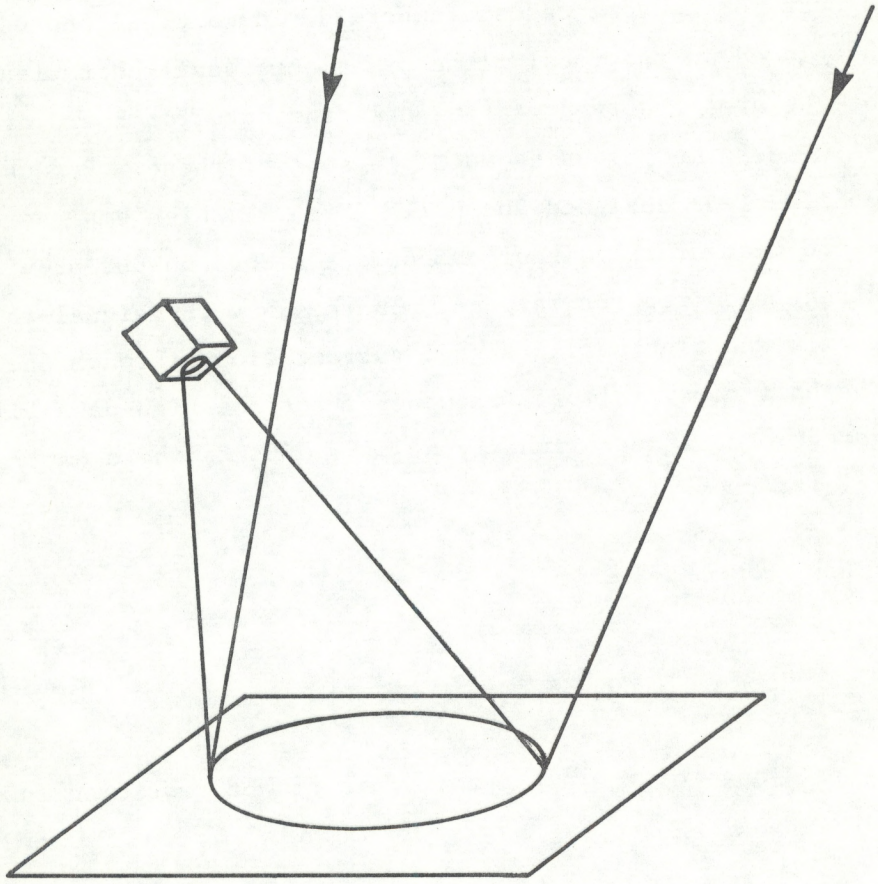

Figure 8. Receiver geometry.

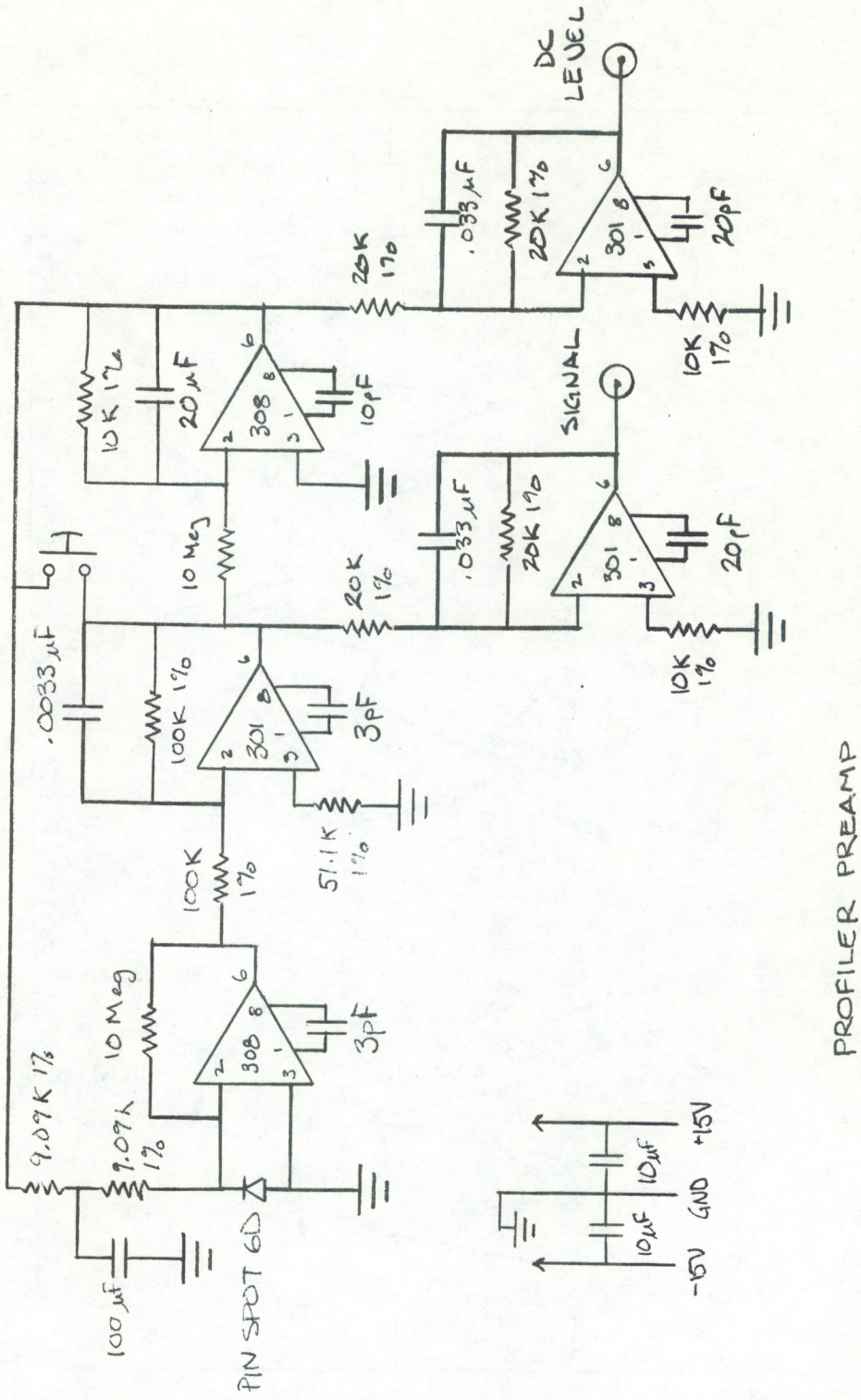

Figure 9. Preamplifier circuit.

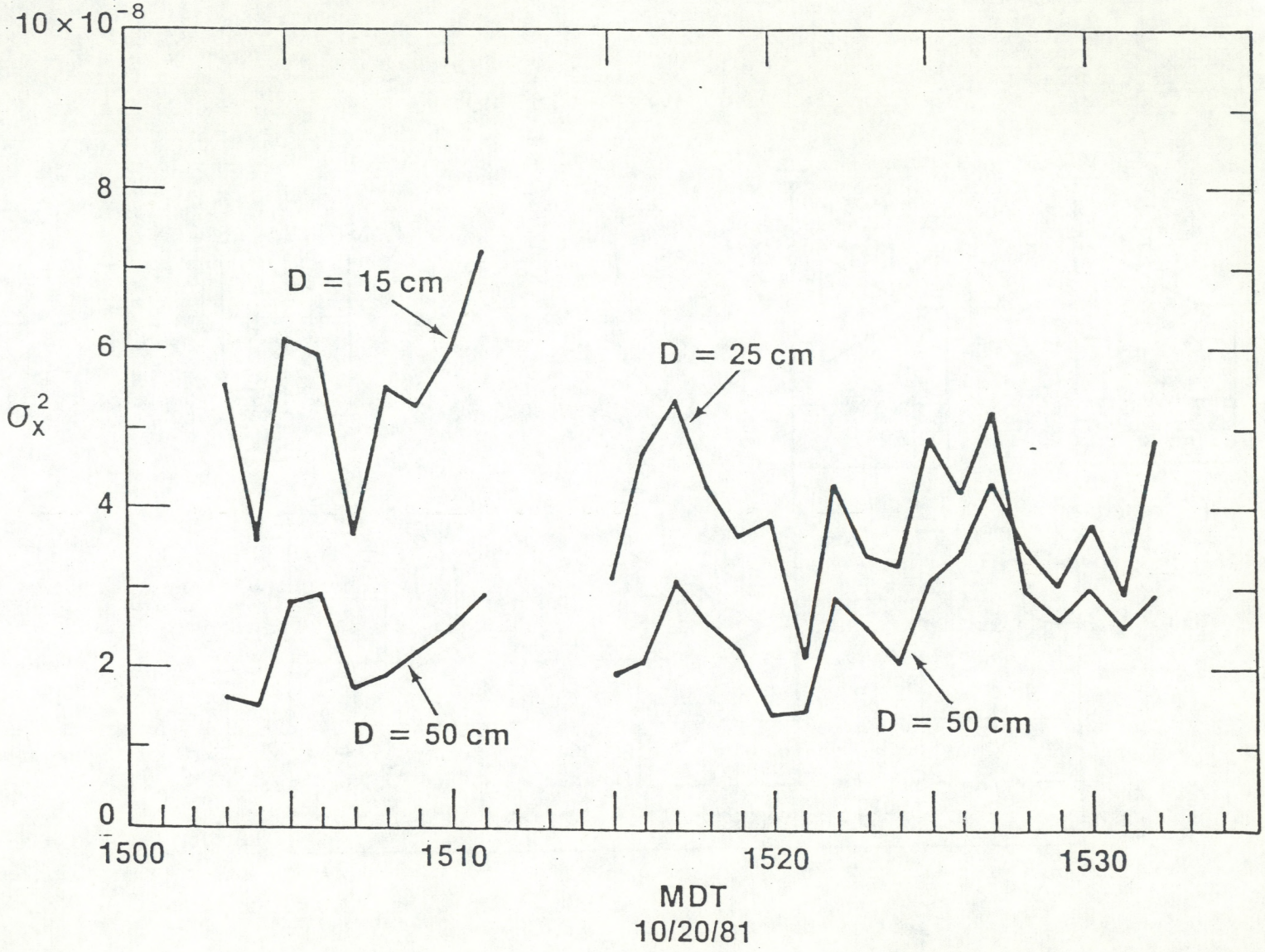

Figure 10. σ_χ^2 *versus time for 15, 25, and 50 cm-diameter apertures.*

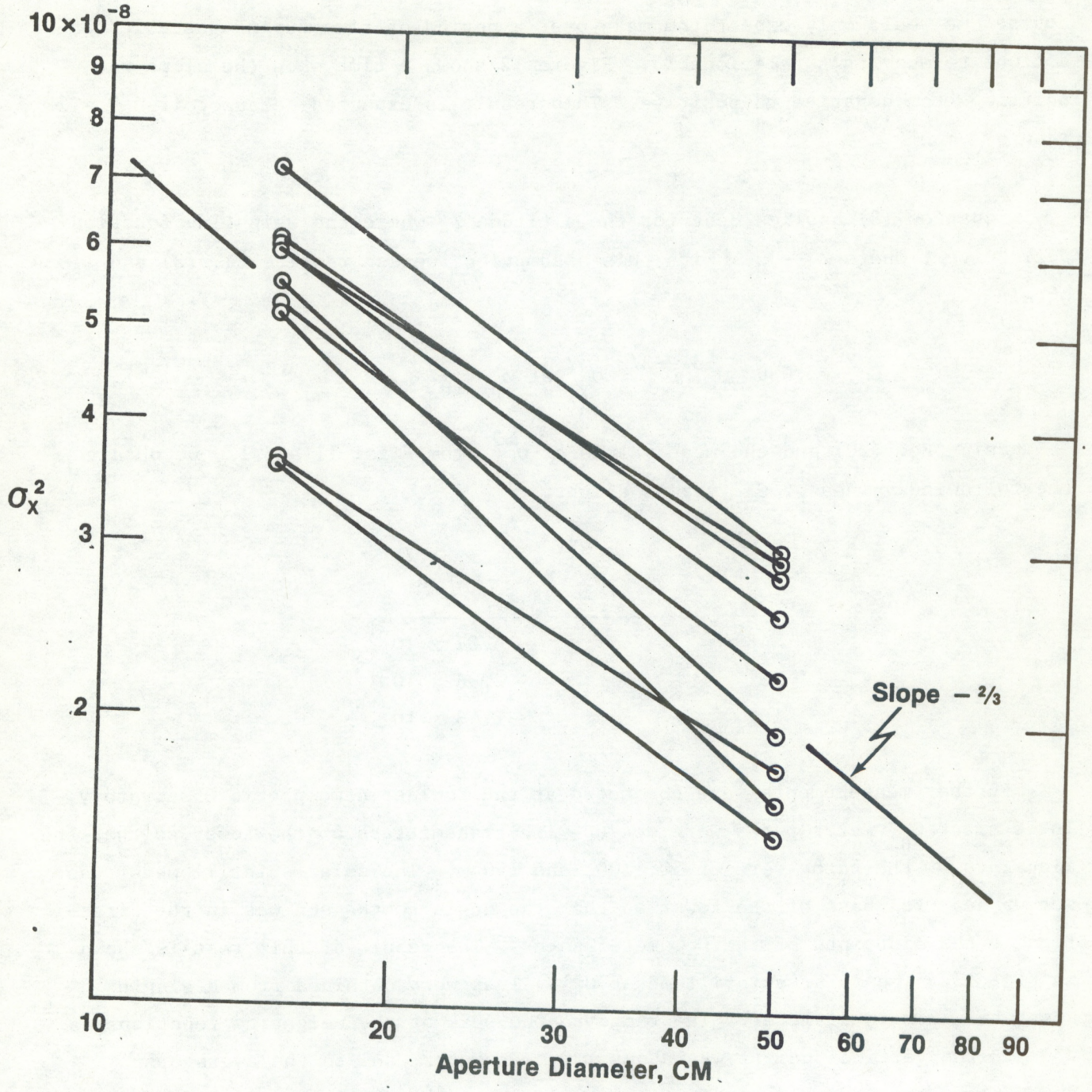

Figure 11. σ_χ^2 *versus 15 and 50 cm-diameter receivers.*

between 1 minute averages of σ_χ^2 taken at the same time for 15 cm and 50 cm diameter apertures. The average agreement with a $D^{-2/3}$ slope is quite acceptable. Of course one would only expect the mean over a period of time during unstable conditions to obey this relationship. Figure 12 shows a time when the slope was shifting from negative to positive. This result is expected because, if $C_n^2 \propto z^{-\nu}$, then $\sigma_\chi^2 \propto D^{2/3-\nu}$.

Equation (8) applies best for the altitude Z_o where the weighting function peaks, i.e., where $Z_p = 3$. With this assumption, we can rewrite Eq. (8) and obtain

$$C_n^2 = .0393\ \theta_s^3\ D^{-2/3}\ \sigma_\chi^2 \text{ at } Z_p = \frac{3D}{\theta_s} \quad . \tag{20}$$

Using Eq. (20) and the mean values of σ_χ^2 from Figs. 11 and 12, we obtain the following values of C_n^2 versus height.

Z_p	C_n^2
48 m	6.07×10^{-15}
81	2.96×10^{-15}
162	1.46×10^{-15}

Further measurements were conducted at the Boulder Atmospheric Observatory. Three slant C_n^2 meter paths were set up with transmitters on the tower so that the midpoints of the paths were at 50, 100, and 150 m. The solar scintillometer was set up near the base of the tower so that the angle to the sun was in the direction of the midpoints of the C_n^2 meter paths. The result of this test is shown in Fig. 13. The solar scintillometer C_n^2 values were obtained from a single aperture .72 m in diameter. The range to the peak of the weighting function was 230 m. The vertical height was about 130 m, however, due to the average sun angle above the horizon at this time. Using Eq. (8) to calculate C_n^2 from σ_χ^2, we find the scintillometer values about a factor of 4 below the C_n^2 meter readings. One possible explanation is that the intensity across the face of the sun and the sensitivity of the receiving aperture both taper from center to edge. Figures 14 and 15 show the distribution of irradiance across the diameter of the sun,[24] and the measured sensitivity of our receiving aperture.

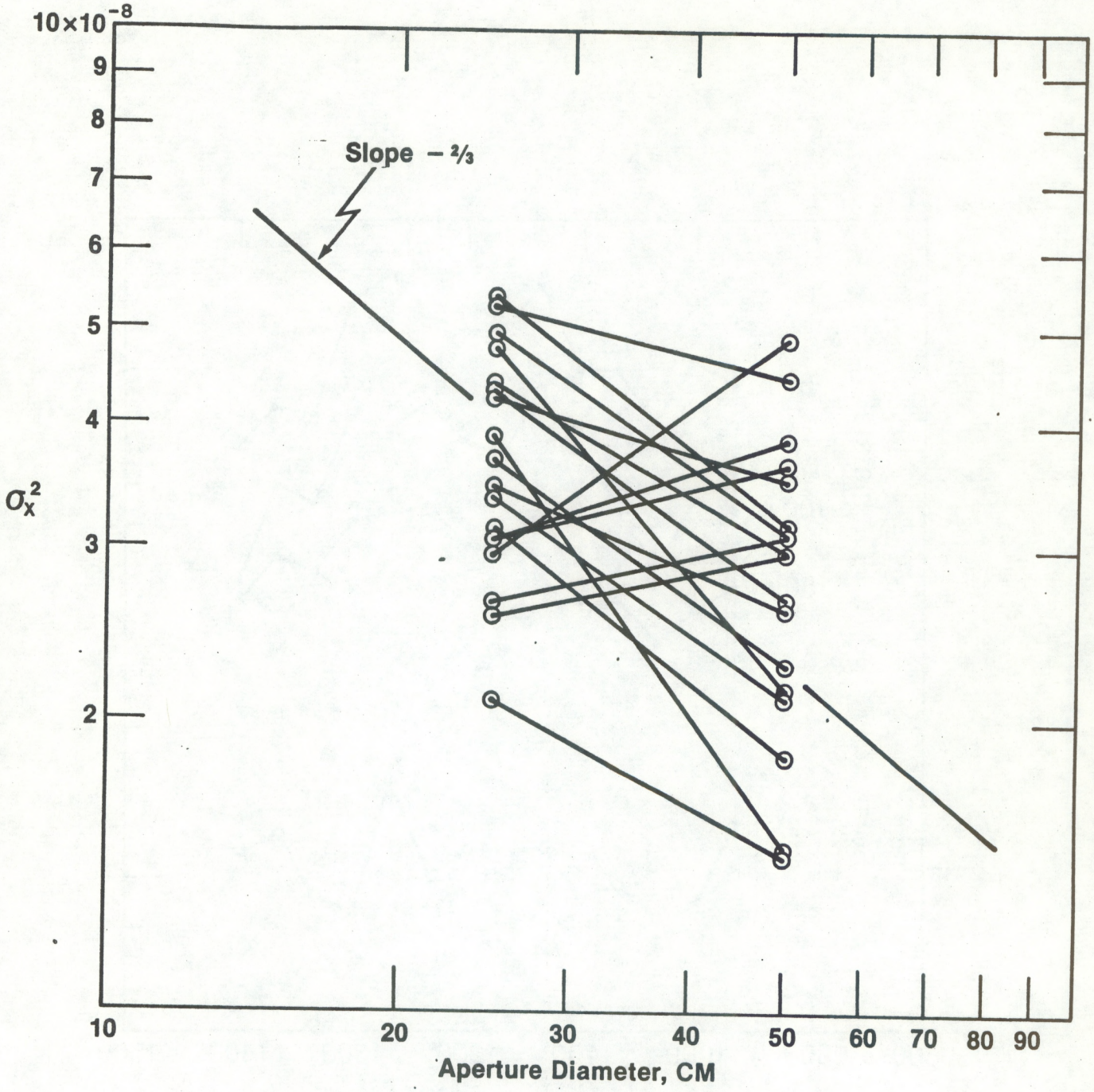

Figure 12. σ_χ^2 *versus 25 and 50 cm-diameter receivers.*

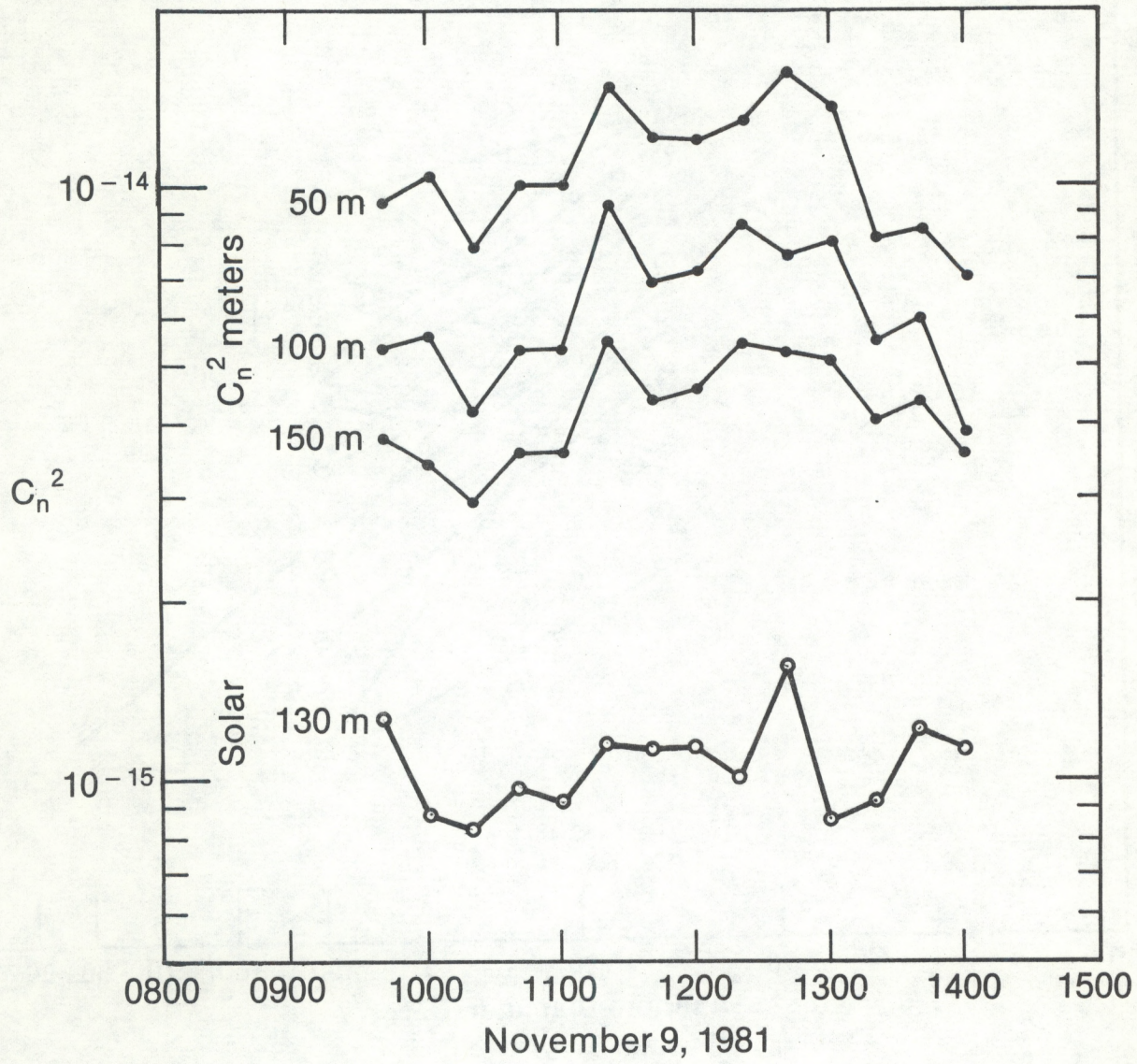

Figure 13. Comparison of C_n^2 derived from the solar scintillometer, and values obtained from three slant-path C_n^2 meters.

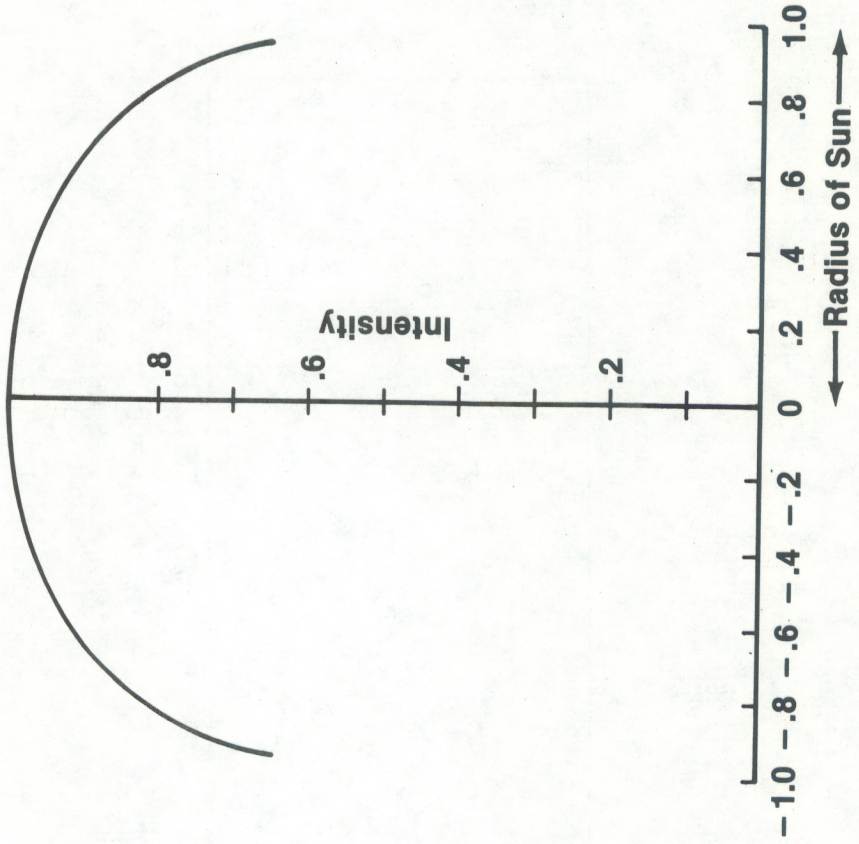

Figure 14. Distribution of irradiance across the sun.

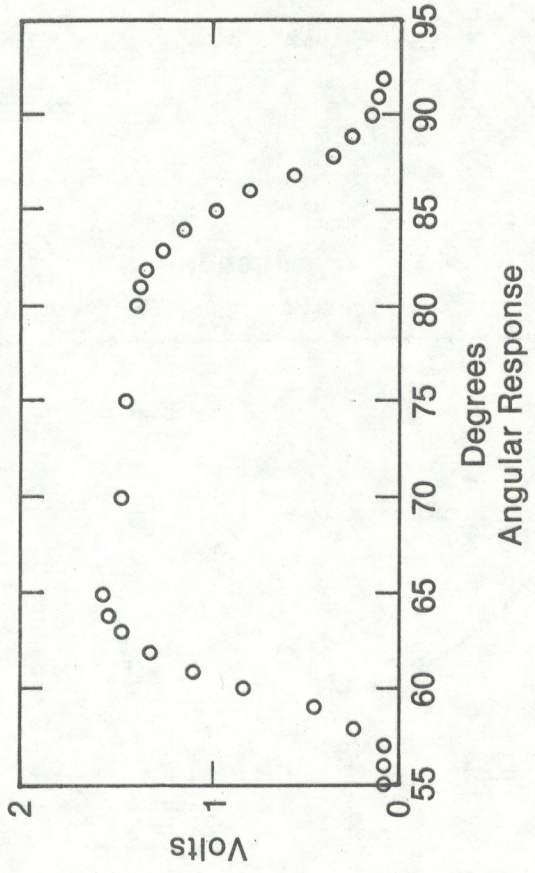

Figure 15. Measured sensitivity over the receiving aperture.

Previous calculations, postulating a solar source with a Gaussian intensity distribution, and a receiver with sensitivity across its aperture according to a Gaussian, show that σ_χ^2 is about 1/5 that for sharp-edged, circular apertures of uniform intensity and sensitivity, with diameters equal to the separation of the $1/e^4$ points on the respective Gaussians. In fact, a known taper in receiver sensitivity may be desirable in that it is more immune to noise generated by movement of the receiver or small moving objects within the field of view.

As the sun angle changes, both the altitude of the measurement and the effective aperture size changes. No correction has been made for these effects in Fig. 13. An approximate calculation shows that if these effects were taken into account to normalize the measurement to a fixed aperture size and height, the plot in Fig. 13 would not change significantly except after 1300, when it would decrease gradually to about 0.6 of the plotted value at 1400. Thus the corrected value would be more in line with the decreasing C_n^2 meter values at this time.

We carried out a separate series of experiments at the Boulder Atmospheric Observatory to measure wind with the solar scintillometer. Two apertures tangent or nearly so, and separated along the direction of the wind, have a time-delayed correlation of the fluctuations in irradiance. A measured function is shown in Fig. 16. We employed the slope system to measure wind, according to the previous analysis. For the apertures used, and the sun angle at the time, the half-power range of the weighting function shown in Fig. 6 (dashed line) is from 20 to 70 m. Considerable response can occur outside this altitude range, though, depending on the actual C_n^2 profile.

The measurements show general agreement with the average of BAO tower wind measurements over the predicted altitude ranges. Figures 17, 18, and 19 are comparisons for the period 0930-1230, October 1, 1981. The wind component at 8 tower levels is plotted, along with the same wind component as calculated from the solar scintillometer, using slightly overlapping apertures 0.5 m in diameter. Figures 20 and 21 are correlation functions averaged over 80 second periods around the times listed. Although more data will be required to obtain an experimental weighting function, the results do not disagree with the prediction. Note how the correlation functions reverse delay with changing wind direction and especially

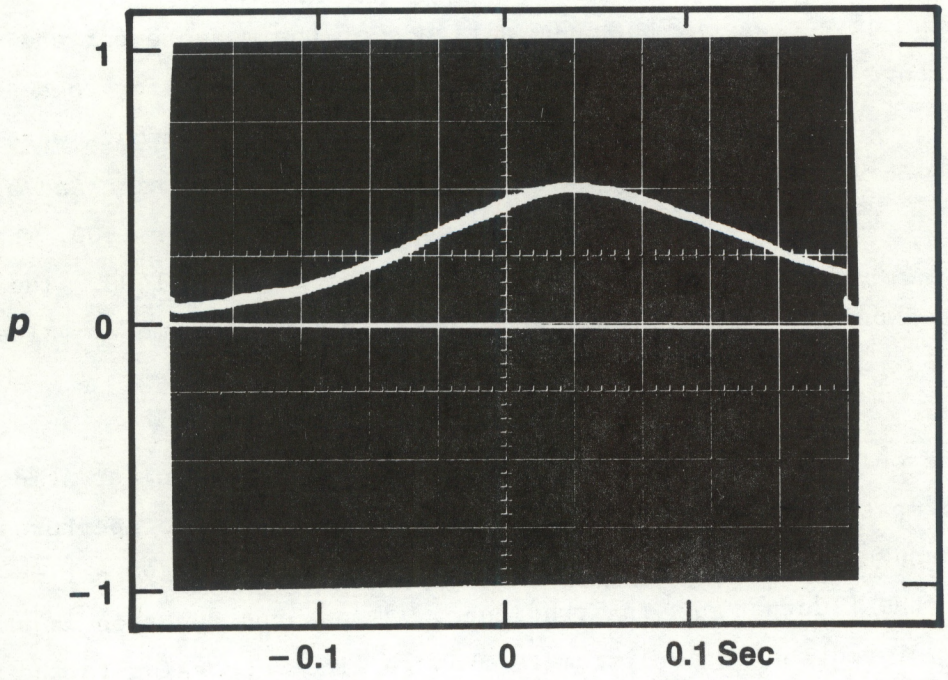

Figure 16. Measured correlation function for two slightly overlapping apertures.

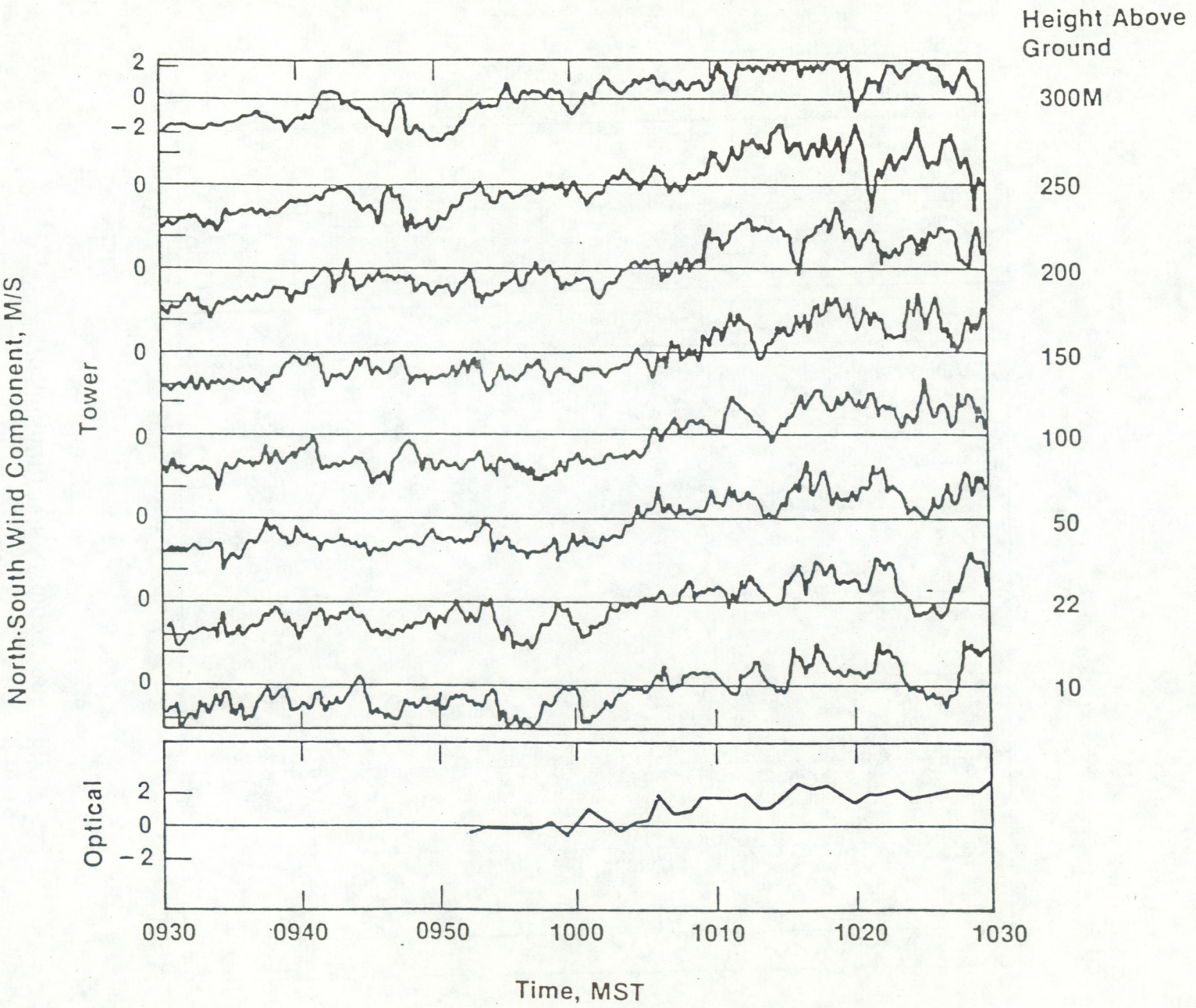

Figure 17. Comparison of solar scintillometer and tower wind measurements. 0930-1030 MST.

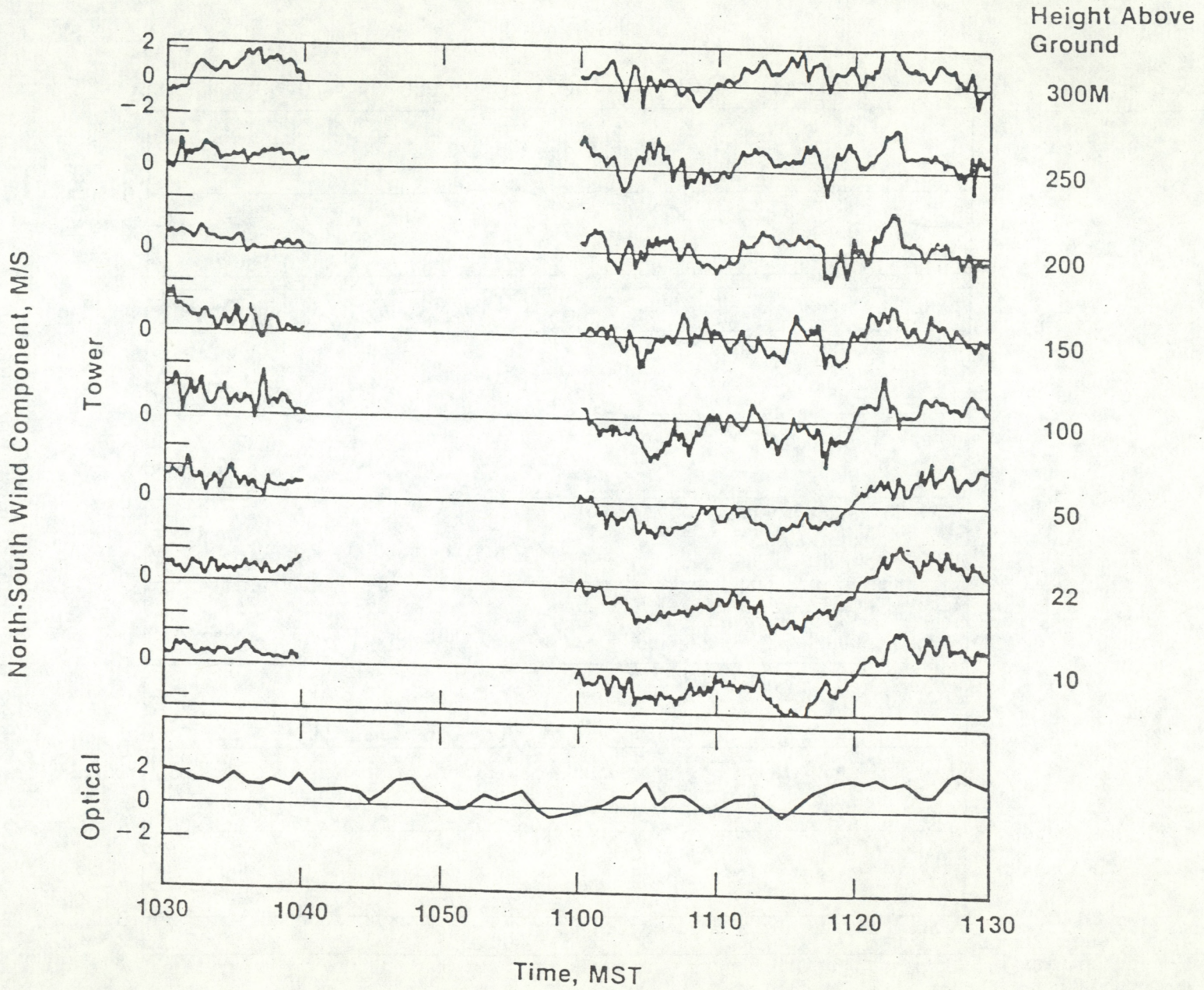

Figure 18. Comparison of solar scintillometer and tower wind measurements. 1030-1130 MST.

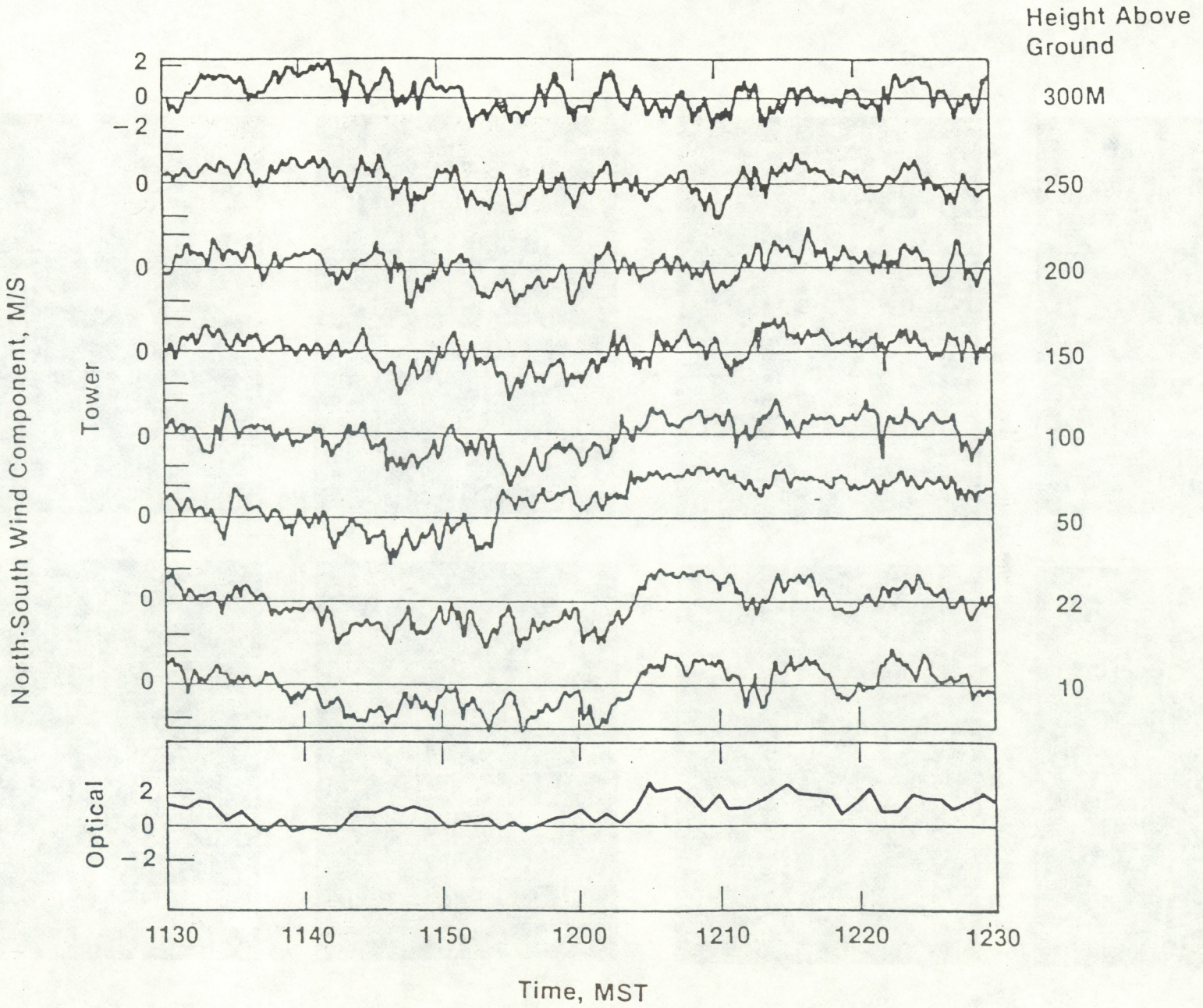

Figure 19. Comparison of solar scintillometer and tower wind measurements. 1130-1230 MST.

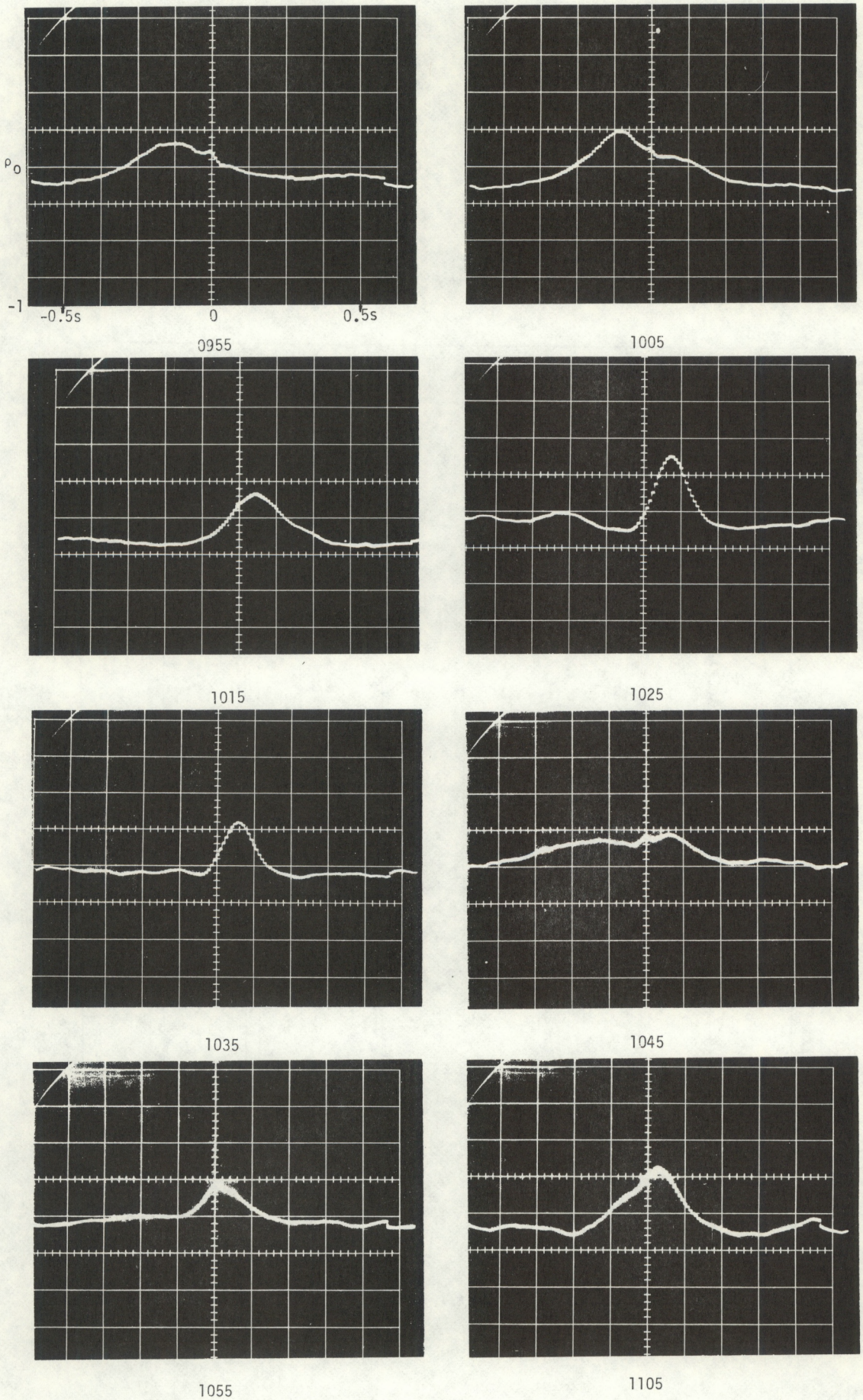

Figure 20. Solar scintillometer correlation functions. 0955-1105 MST.

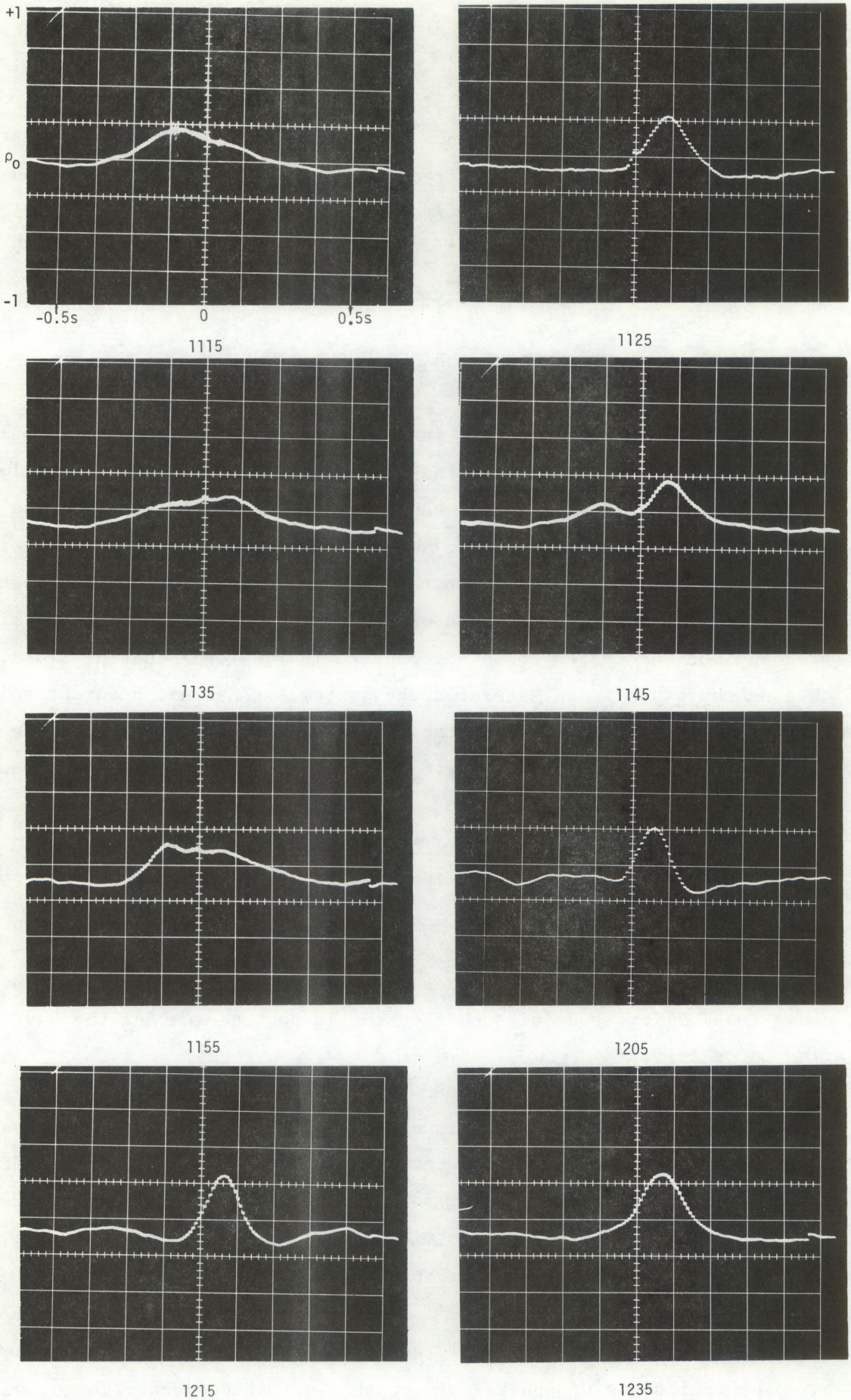

Figure 21. Solar scintillometer correlation functions. 1115-1235 MST.

note the two-humped functions from 1135 to 1155, which clearly show the oppositely directed winds at low and high altitude. The negative portions of the covariance functions clearly indicate a narrower frequency band than would be expected from the theory. This was due to decreased frequency response in the preamplifiers below 14 Hz.

CONCLUSIONS AND RECOMMENDATIONS

The solar scintillometer study so far indicates that an instrument could be designed to profile C_n^2 and wind from the ground to a height of several kilometers over a four hour period around noon on sunny days. Signal fluctuations due to high cloudiness and fluctuations due to aerosols nearer the ground are major problems, though. Both of these affect the C_n^2 measurement to a greater extent than the wind measurement. The effects of faint high cloudiness could be minimized by differencing but the system could not operate in low-level dust or smoke. While dust from a nearby gravel road saturated the system, it has not been determined whether normal atmospheric aerosol content has a serious effect. In this case we would expect too large an answer for C_n^2, and the test results do not support this. The method remains attractive but more observations need to be taken. We recommend that a prototype system be built to process the data on line. This would allow us to compare data against tower measurements over a longer period of time for a better evaluation.

There is a distinct possibility that a lidar system could obtain C_n^2 profiles, and a feasibility study of such a system is now underway at the Wave Propagation Laboratory.

The above approaches should be pursued. The solar scintillometer is potentially a rather simple system, easy to set up, and it lends itself to simultaneous observations at more than one location, for better site comparison. On the other hand, the lidar system would not be restricted as to time of operation, and continuous day and night observations could be made.

There are other methods that should be considered that are available now or nearly so. The radiosonde C_t^2 package is capable of making measurements over the

entire useful altitude range and could be used by itself or in conjunction with other methods. Of course only a limited amount of data can be accumulated over a period of time. The optical C_n^2 meter should be considered as a supplementary system to operate continuously at selected sites.

Rather than obtaining a C_n^2 profile, one could concentrate on measuring atmospheric quantities directly related to image quality, by using the Walters star trail system or developing an isoplanometer as discussed by Loos and Hogge. We summarize the results in Table III.

ACKNOWLEDGMENTS

We acknowledge the helpful discussions with Ting-i Wang and R. J. Hill regarding the solar scintillation theory. We are indebted to R. L. Schwiesow for all of the information regarding the new lidar technique. J. T. Priestley calculated all of the weighting functions in this paper, as well as many others that contributed to a better understanding of the project.

Table III

Technique	Quantities Measured	Time of Measurement	Status
Radiosonde with C_t^2 package.	Profiles wind, C_n^2 from C_t^2 profile over entire altitude range.	Limited number 24 hrs a day except during high winds.	Essentially available now.
Optical C_n^2 meter	C_n^2, horizontal line average.	24 hrs a day.	Available now.
Walters star trail system.	r_o (coherence diameter).	24 hrs a day (1st magnitude stars daytime, 1st and 2nd magnitude at night).	System is operational. Building a system would require co-operation of Atmospheric Sciences Lab, White Sands Missile Range.
Isoplanometer	σ_χ^2, 10 cm aperture, from which derive θ, the isoplanatic angle. All-atmosphere measurement.	24 hrs a day (1st magnitude stars daytime, 1st and 2nd magnitude at night).	Theory is worked out. Feasibility shown experimentally using too large aperture (36 cm).
Solar scintillometer	Profiles wind and C_n^2 to estimated 3 km range.	Limited to approximately 4 hrs around noon.	Theory is worked out. Experimental comparisons made to 300 m height.
Lidar	Profiles C_n^2 and wind.	24 hrs a day.	A feasibility study is underway.

REFERENCES

1. Fried, D.L., Remote probing of the optical strength of atmospheric turbulence and of wind velocity, Proc. IEEE, 57, April 1969.

2. Ochs, G.R., Ting-i Wang, R.S. Lawrence, and S.F. Clifford, Refractive-turbulence profiles measured by one-dimensional spatial filtering of scintillations, Appl. Optics, 15, 2504, Oct. 1976.

3. Wang, Ting-i, G.R. Ochs, and S.F. Clifford, A saturation-resistant optical scintillometer to measure C_n^2, J. Opt. Soc. Am., 68, March 1978.

4. Rocca, A., F. Roddier, and J. Vermin, Detection of atmospheric turbulent layers by spatiotemporal and spatioangular correlation measurements of stellar-light scintillation, J. Opt. Soc. Am., 64, July 1974.

5. Wolf, E. Progress in Optics, Volume XIX, North-Holland Publishing Company - Amsterdam New York Oxford, See Ch. V, F. Roddier, The Effects of Atmospheric Turbulence in Optical Astronomy.

6. Greenwood, D.P., J. Opt. Soc. Am., 67, March 1977.

7. Hufnagel, R.E., Variations of atmospheric turbulence, Digest of Technical Papers, Topical Meeting on Optical Propagation through Turbulence, July 9-11, 1974, Univ. of Colorado, Boulder, Colorado.

8. Walters, D.L., and K.E. Kunkel, Atmospheric modulation transfer function for desert and mountain: the atmospheric effects on r_o, J. Opt. Soc. Am. 71, April 1981.

9. Walters, D.L., Atmospheric modulation transfer function for desert and mountain locations: r_o measurements, J. Opt. Soc. Am. 71, April 1981.

10. Nastrom, G.D., K.S. Gage, and B.B. Balsley, The variability of C_n^2 at Poker Flat, Alaska, from MST Doppler radar observations, SPIE Proc. 277.

11. Ochs, G.R., B.W. Guderian, and W.D. Cartwright, Fine-wire instruments for measuring the temperature structure parameter, NOAA Tech. Memo., in process.

12. Fritz, R.B., and R.S. Lawrence, WSMR Atmospheric Structure Constant (C_n^2) Survey, NOAA Tech. Memo ERL WPL-27.

13. Walters, D.L., D.L. Favier, and J.R. Hines, Vertical path atmospheric MTF measurements, J. Opt. Soc. Am., 69, June 1979.

14. Walters, D.L., Private communication.

15. Loos, G.C., and C.B. Hogge, Turbulence of the upper atmosphere and isoplanatism, Appl. Optics, 18, 1 August 1979.

16. Borgnino, J., and F. Martin, Correlation between angle-of-arrival fluctuations on the entrance pupil of a solar telescope, J. Opt. Soc. Am., 67, August 1977.

17. Borgnino and J. Vermin, Experimental verification of the inertial model of atmospheric turbulence from solar limb motion, J. Opt. Soc. Am., 68, August 1978.

18. Wessely, H.W., and M.P. Mitchell, Solar-scintillation measurements, J. Opt. Soc. Am., 61, February 1971.

19. Wolfe, W.L., and G.J. Zissis, Editors, The Infrared Handbook, Office of Naval Research, Dept. of the Navy, Washington, D.C. (See Chapter 6 by Robert E. Hufnagel.)

20. Clifford, S.F., G.R. Ochs, and T-i Wang, Optical wind sensing by observing the scintillations of a random scene, Appl. Optics, 14, Dec. 1975.

21. Tatarski, V.I., The effects of the turbulent atmosphere on wave propagation, National Technical Information Service, Springfield, VA, 1971.

22. LaBonte, B.J., and R. Howard, Measurement of solar radius changes, Science, 214, 20 November 1981.

23. Lawrence, R.S., G.R. Ochs, and S.F. Clifford, Use of scintillations to measure average wind across a light beam, Appl. Optics, 11, 239, 1972.

24. Kuiper, G.P., Editor, The Sun, The Univ. of Chicago Press, Chicago, Illinois.